AMERICAN UNIVERSITY OF BEIRUT

A MICROFLUIDIC TRANSISTOR FOR ANALOG MICRO-FLOWS CONTROL

by

MOHAMAD IBRAHIM CHEIKH

A thesis
submitted in partial fulfillment of the requirements
for the degree of Master of Engineering
to the Department of Mechanical Engineering
of the Faculty of Engineering and Architecture
at the American University of Beirut

Beirut, Lebanon
April 2015

AMERICAN UNIVERSITY OF BEIRUT

A MICROFLUIDIC TRANSISTOR FOR ANALOG MICRO-FLOWS CONTROL

by

MOHAMAD IBRAHIM CHEIKH

Approved by:

_____   Advisor

Issam Lakkis, Associate Professor
Mechanical Engineering

_____   Committee Member

Fadl Moukalled, Professor
Mechanical Engineering

_____   Committee Member

Mu'tasem Shehadeh, Assistant Professor
Mechanical Engineering

Date of thesis defense: 04/05/2015

AMERICAN UNIVERSITY OF BEIRUT

THESIS, DISSERTATION, PROJECT RELEASE FORM

Student Name: _____Cheikh_____Mohammad Ibrahim_____Nabil___

                              Last   First   Middle

◯ Master's Thesis   ◯ Master's Project   ◯ Doctoral Dissertation

☐   I authorize the American University of Beirut to: (a) reproduce hard or electronic copies of my thesis, dissertation, or project; (b) include such copies in the archives and digital repositories of the University; and (c) make freely available such copies to third parties for research or educational purposes.

☐   I authorize the American University of Beirut, **three years after the date of submitting my thesis, dissertation, or project,** to: (a) reproduce hard or electronic copies of it; (b) include such copies in the archives and digital repositories of the University; and (c) make freely available such copies to third parties for research or educational purposes.

_____

Signature   Date

ACKNOWLEDGEMENTS

AN ABSTRACT OF THE THESIS OF

Mohamad Ibrahim Cheikh   for   Master of Engineering
                                      Major: Mechanical Engineering

Title: A Microfluidic Transistor for Analog Micro-Flows Control

In this work, a microfluidic device for analog flow control is presented. The device consists of a microchannel with an elastic compliant wall where the fluid flow-rate is controlled by the combined effect of the pressure differential across the channel and the deflection of the elastic wall. A reduced-order model that captures the steady and low-frequency unsteady behavior of the device is presented. The model is based on coupling the equations governing the membrane deflection and fluid flow while employing some assumptions to reduce their complexity. Numerical simulations ANSYS-Fluent are used for characterizing the device behavior in terms of dependence of the flow rate on the operating pressure differences; in a manner analogous to analogous to standard characterization of electronic transistors. In addition to the characteristic curves, the reduced order parameters (i.e. the fluidic transconductance, intrinsic output resistance, and gain) are generated over wide ranges of operating pressures. Accuracy of the proposed reduced-order model is assessed by comparing with ANSYS fluid-structure interaction (FSI) simulation. Finally an applications of how the transistor can be used is presented in for two examples: (i) in a common source circuit configuration for small signal amplification, and (ii) as an analog flow controller for mixing of two pulsating flows.

CONTENTS

ILLUSTRATIONS

TABLES

Nomenclature

$\dot{m}$	Mass flow rate
t	time
f	frequency
μ	Viscosity of the fluid
E	Modulus of elasticity
A	Cross Sectional Area
L	Length of fluidic transistor
L_c	Length of channel before fluidic transistor
h_0	Refence channel height of undeflected transistor channel
W	Width of fluidic transistor
ρ	Density
d	Thickness of the gate
δ	Vertical deflection of the gate from equilibrium
δ_c	Vertical deflection at the center of the gate
u	Velocity of fluid in the x direction
U_x	Average Velocity of fluid in the x direction
v	Velocity of fluid in the y direction
U_y	Average Velocity of fluid in the y direction
w	Velocity of fluid in the z direction
U_z	Average Velocity of fluid in the z direction
Q	Volume flow rate
g_m	Transconductance
r_o	Intrinsic output resistance
A_v	Intrinsic pressure gain
p	Pressure inside the channel
p_d	Inlet pressure of the fluid
p_s	Outlet pressure of the fluid

p_g	External pressure above the gate
p_{ds}	Pressure drop from input to output
p_{gs}	Actuation Pressure relative to output pressure
U_{pois}	Average speed of a Poiseuille flow in a channel with reference pressure $p_{ds,0}$.
U	Reference speed $= 12U_{pois}$.
ν	Kinematic viscosity
Re	Reynolds number
St	Strouhal number
α	Transistor channel aspect ratio
$(.)_0$	Refers to reference or DC state
$(.)_{DC}$	Refers to reference or DC state
$(.)_f$	Refers to fluid
$(.)_m$	Refers to membrane
$(.)_g$	Refers to the gate

CHAPTER I

INTRODUCTION

An important aspect of microfluidics is the ability to control flow movement inside microchannel networks [15, 25]. Many methods have been developed to control flow in microfluidic channels. One method requires the use of complex active controllers that are conducted off-chip either manually or electronically [25]. These devices grant an organised control of the fluids spatial and temporal parameters. Examples of such control systems are the syringe pump and the pressure regulated manifolds. Although they are easy to use, but these systems are tiresome, expensive and have limited flow control; there is no ability to dynamically reroute fluids. Other methods involve electroosmosis [18] and passive surface tension pumping [5]. Electro-osmosis is generated when a two layers of electric charges form at the channel walls , due to an electric field, this duality causes movement of charges toward the opposite charge. This movement of charges will cause a bulk movement in the fluid near the wall in due to viscous forces. While this method causes a uniform velocity profile inside the channel however due to the electro-chemical interactions with proteins and biomaterails in the solutions makes it laborious to implement in biotechnology [15]. Surface tension pumping, on the other hand, uses the intrinsic disparity in surface tension between droplets of different diameters to induce a movement from the small to the large droplet. The advantage of such a method is that it is completely passive Yet, its only limited to small amounts of liquid making the flow profile limited and transient [15].

A. Introduction to Elastomeric-Membrane Component

In order to reduce the quantity of external instrument needed to control flow in a microfluidic devices, embedded elements have been designed to provide automatic feedback for any pressure or flow changes for Lab on-chip devices [1, 26]. One component in such circuits that is gaining increasing attention is the elastic membrane micro channel which is made up of elastomers, particularly polydimethylsiloxane (PDMS) [6]. Although hard materials like silicon and glass where the origin of microfluidic devices, these materials are expensive, arduous to manufacture, and have many disadvantages when working with biomaterials [25]. Therefore, elastomers which are cheap, biocompatible, and provide an ease in manufacturing have become the base materials for rapid prototyping in microfluidics. Specially, Polydimethylsiloxane (PDMS) due to its translucent property, high porosity for gases, biocompatiblity, and capability to affix to other different type of layers to form microfluidic structures [25].

The basic procedure in the fabrication of microfluidic devices with elastromeric component is to start with a permanent mold [25]. These molds are developed by photolithography, a process that uses ultraviolet light to convey a geometric pattern from a photomask to a light-sensitive photoresist chemical on a silicon wafer. Once finished a mixture of PDMS oligomers and curing agent are added to the silicon wafer and heated afterwards. Finally the PDMS stiffness is modified through varying the ratio of oligomer and curing agent, and its surface hydrophilicity is altered to bond better with various materials through exposing it to plasma treatment.

B. Elastomeric-Membrane Based Microfluidic Systems

For the most part, elastomeric components have been used as valves or switches, where a pressure difference across the flexible membrane causes a downward deflection of the membrane that changes its state from open to closed, thus blocking any

flow from passing[8]. These elastomeric components are commonly made of two thick stiff layers sandwiching a thin flexible membrane usually made of elastomers, particularly polydimethylsiloxane (PDMS) [7]. In kim [10] the authors used the elastic membrane as a switch to create an oscillating flow inside the micro fluidic circuit. Kim [10] related the behaviour of his valve to the electric transistor MOSFET where he controlled the opening and closing of his valve through varying the pressure at the membrane with respect to the pressure of the flow. However kim didn't fully study the full behavior of his device and how close is it to the transistor.

Another method reported in the literature, uses these elastic membranes, not as a valve, but as a means to alter the geometries of the microchannel in response to a pressure changes [9]. The significance of this method is that it gave the fluids in a microfluidic devices the ability to self-regulate by distributing pressure fields acting on the membrane. Mosadegh [12] used this approach to introduce to control the flow, and related their behavior to the electric diode and and p-channel JFET transistor as shown in Fig.1. Using theses two devices Mosadegh was able to create an oscillating flow dependent on the pressure distribution of the fluid. However, like the valves described before, these two method have no systematic switching mechanisms that can suffice as a fully functioning control system.

Leslie [11], on the other hand described the use of elastomeric membrane as capacitors not valves, since they held capability for deforming and storing mass inside them similar to an electric capacitor thats able to stores energy as shown in Fig.2. Leslie was able to build a fluidic circuit that was able to selectively transport the fluid in response to the frequency of a single external time-modulated pressure source [11]. Using this method [11] was able to show that different flow patterns could be achieved with different actuation frequencies. This strategy diminishes the need for a large number of actuators and shifts the control to frequency actuation. Moreover [11] provided a linearized model for the capacitive behavior of the device that relates the
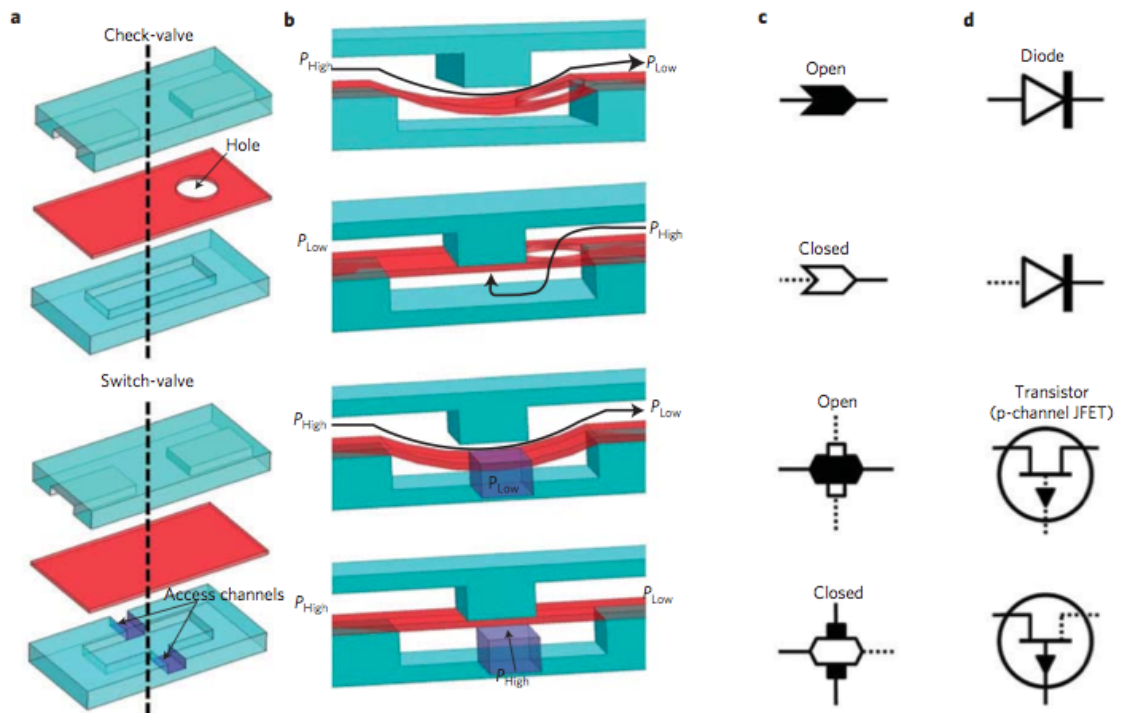
Figure 1: **a**, A three-layer composite of the check-valve and switch-valve. **b**, Cross-section schematic of the check-valve and switch-valve. **c-d**, Corresponding symbolic and electric analogies of the check-valve and switch-valve. Taken from [12]

mass flow rate to the time rate of change of pressure difference across the capacitor by a proportionality constant that is known as the fluidic capacitance. This simple model does not, however, cover the full functional regimes of the component performance.

As Mosadegh [13] states, there is a need to control the output flow of a certain fluidic network using minimal input actuators to save space and energy. Hence the use of logic based fluidic circuits enables the user to control a large number of output flows with minimal input gates. In addition, there is the need for simple means to translate an input electric signal to an input fluidic signal without the use of electromechanical interface actuators[13]. The need for a large number of actuators is a problem especially when designing large integrated micro-fluidic circuits. A solution, proposed by Leslie [11] is to build fluidic networks with elastomeric components that selectively transport the fluid in response to the frequency of a single external time-modulated pressure source.This strategy diminishes the need for a large number of actuators and shifts the control to frequency actuation. Similar device has also been used as a switch to model microfluidic

6
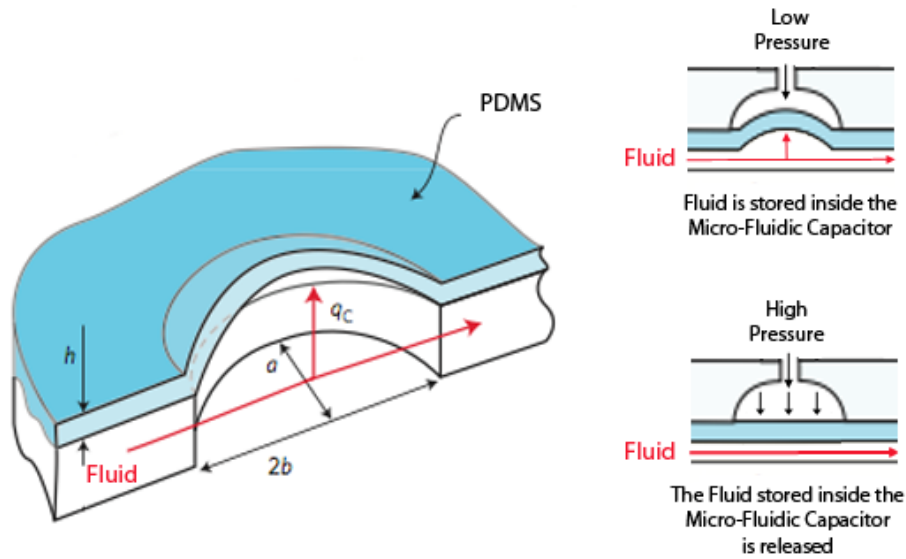
Figure 2: Design of the fluidic capacitors used by [11]. This devices stores and releases fluid (volumetric flow rate) in proportion to the time rate of change in pressure inside the network

logic circuits [21, 16, 24, 22], where transistor-like elements operating as logic switches are employed as the basic building blocks for their logic circuits. In [22] the authors have used passive pumping techniques to construct a set of basic logic gates that serve as building blocks for larger circuits. In [16] the transistors were pneumatically driven, while in [24] they were fluid driven. As an alternative to pressure-based actuation, electrostatic actuation was proposed in [?] to deform the membrane for flow control.

C. Models in the Literture

Analogies between electric and fluidic components have been extensively used in fluidic circuit analysis [14]. The motivation behind this analogy is that the analysis of large networks of fluidic circuits is made simpler by using well established techniques in electric circuit analysis. While successful component design requires accurate characterization of the device behavior over the intended regime of operation, design and integration of a large microfluidic circuit requires accurate reduced-order models of the

components behavior that can be used in large circuit design environment tools. Leslie's [11] capacitive model relates the flow rate coming out of the capacitor to the pressure difference acting on the film $q = C(p_{ext} - pin)$ where the capacitance is a function of the deflection and pressure. In his model Leslie used electric circuit analogies to relate the frequency response of his capacitor to its dimensions. Wobschall [**?**] goes further into characterising the frequency response of the capacitive behavior of an elastic bilayer by accounting some of the physical limitations such as breakage at the boundary between the membrane and the solid wall, thinning and stretching of the elastic membrane.A linearized model of the dynamic behavior of a piezoelectric actuated diaphragm micro pump is presented in [2]. A linearized dynamic system model of actuated micropump is developed in [2] using electric circuit analogies. A model that couples the pressure waves in the fluid to the bending waves of a passive elastic membrane in a ling channel is presented in [23].

Although these components can be found frequently in the literature[11, 21, 16, 12, 24], a reduced order model that captures the dynamic behavior over wide ranges of operating parameters is still lacking. Such a model predicts the dynamic dependence of the flow rate on geometric parameters, physical properties, pressure drop along the channel, in addition to the external actuation force. Furthermore, focus has so far been on the capacitive behavior of the device for charging and discharging mass.

The elastic membrane micro-channel has the potential to revolutionize the micro-fluidics industry. To realize that potential, new regimes of operation of this versatile device need to be uncovered, in addition to thorough characterization of the dynamic and static behavior of the device, followed by development of reduced order models to allow fast design and simulation of large microfluidic networks.
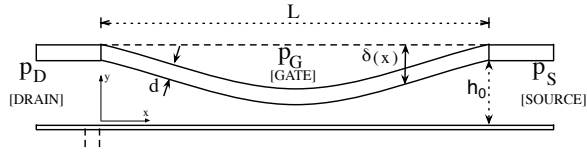
Figure 3: Schematic of the microfluidic transistor.

D. Thesis Contribution

In this work, we present a novel regime of the elastic membrane microchannel; as a microfluidic transistor for analog flow control. The transistor, depicted in Fig. 3, consists of a microchannel with a compliant wall where the fluid flow-rate is controlled by the combined effect of the pressure differential across the channel $(p_d - p_s)$ and the upper wall deflection (δ) controlled by the external pressure (p_g). Delivering a flowrate (current) to the load takes place through the dashed channel at the drain. A reduced-order analytical model that captures both the steady, and the low-frequency behavior of the device is presented in Sec. II. The model is based on coupling the equations governing the membrane deflection and fluid flow while employing some assumptions to reduce their complexity. Sec. III discusses the numerical method to implement the model.In Sec. IV, numerical simulations ANSYS-Fluent are used for characterizing the device behavior in terms of dependence of the flow rate Q on the operating pressure differences $(p_{ds} = p_d - p_s$ and $p_{gs} = p_s - p_g)$; in a manner analogous to analogous to standard characterization of electronic transistors. In addition to the characteristic curves, the capacitive and reduced order parameters (i.e. the fluidic transconductance, intrinsic output resistance, and gain) are generated over wide ranges of operating pressures. In Sec. V accuracy of the proposed reduced-order model is assessed by comparing with ANSYS fluid-structure interaction (FSI) simulation. Applications of how the transistor can be used are presented in Sec. VI for two examples: (i) exploring the transistor in a common source circuit for small signal amplification, and (ii) using the transistor as an analog flow controller for mixing of two pulsating flows.

9

CHAPTER II

REDUCED-ORDER MODEL

In order to model the microfluidic transistor, the solid mechanics of the membrane should be coupled with the fluid dynamics of the flow. Various models for a fluidic microchannel with a deformable membrane can be found in the literature [4, 19, 3]. In [4], Begley introduces a fourth order polynomial for the deflection of the membrane δ as a function of the average pressure differential across the channel. Begley's model assumes a symmetric membrane with no pressure difference between the input and output of the channel. A model that accounts for the pressure drop along the channel is presented in [3]. The model that uses a trial function for the deflection proposed by Senturia in [19] that automatically satisfies the boundary conditions at both fixed ends, and accounts for both small and large deflections (stretching and bending) at the center. This model, however, only solves for the center deflection which is assumed to be maximum at the middle $\frac{L}{2}$, with the assumption that the pressure distribution under the membrane is uniform. These assumptions contribute to significant departure of the behavior prediced by the analytical model from numerical simulations. In what follows, we present an improved model of the microfluidic transistor that allows for more accurate membrane deflection and flow pressure profiles along the channel.

A. Plate Deflection

Considering an isotropic homogeneous thin plate clamped at its boundary, the deformation (measured upwards) is governed by[20]

$$D\nabla^2\nabla^2\delta + c\frac{\partial\delta}{\partial t} + \rho_m d\frac{\partial^2\delta}{\partial t^2} = p(x,t) - p_g + N_x\frac{\partial^2\delta}{\partial x^2} + N_z\frac{\partial^2\delta}{\partial z^2} - 2N_{xz}\frac{\partial^2\delta}{\partial x\partial z} \quad (1)$$

where

$$\nabla^2\nabla^2\delta = \frac{\partial^4\delta}{\partial x^4} + 2\frac{\partial^4\delta}{\partial x^2\partial z^2} + \frac{\partial^4\delta}{\partial z^4}, \quad (2)$$

$p(x,t)$ is the pressure exerted on the plate by the fluid in the channel, p_g is the pressure applied externally on the other (gate) side of the plate, δ the mid-plane deflection in the direction normal to the flow, D is the flexural rigidity ($D \equiv Ed^3/(12(1-v^2))$), c is the damping coefficient, ρ_m is the density, d is the plate thickness, and N_x, N_z and N_{xz} are the in-plane stretching stresses, expressed in terms of the strains as

$$N_x = \frac{Ed}{1-v^2}(\varepsilon_x + v\varepsilon_z) \quad (3)$$

$$N_z = \frac{Ed}{1-v^2}(\varepsilon_z + v\varepsilon_x) \quad (4)$$

$$N_{xz} = Gd\gamma_{xz} \quad (5)$$

Assuming the plate width (normal to flow) is much larger than its length (along the flow), $W/L \gg 1$, strains in the $z-$ direction can then be neglected, so that $\varepsilon_z = 0$ and $\gamma_{xz} = 0$ (plane strain). This implies that the displacement in the z direction is zero, $\delta_z = 0$, and the displacements in the x and y directions do not depend on z, i.e. $\partial\delta_x/\partial z = \partial\delta_y/\partial z = 0$. Noting that $\delta \equiv \delta_y$,

$$N_x = \frac{Ed}{1-v^2}\varepsilon_x = \frac{Ed}{1-v^2}\left(\frac{\partial\delta_x}{\partial x} + \frac{1}{2}\left(\frac{\partial\delta}{\partial x}\right)^2\right) \quad (6)$$

Upon employing the equations of equilibrium of an element in the $x - z$ plane, we get

$$\frac{\partial N_x}{\partial x} = 0 \tag{7}$$

so that the stretching force is independent of x and is expressed as

$$N_x = \frac{Ed}{2(1-v^2)L} \int_0^L \left(\frac{\partial \delta}{\partial x}\right)^2 dx \tag{8}$$

The equation governing the deflection of the plate is then

$$D\frac{\partial^4 \delta}{\partial x^4} + c\frac{\partial \delta}{\partial t} + \rho_m d\frac{\partial^2 \delta}{\partial t^2} = p - p_g + N_x\frac{\partial^2 \delta}{\partial x^2} \tag{9}$$

Scaling δ by a reference channel height, h_0, x by channel length, L, t by $1/f$, where f is a reference frequency of the forcing (pressure at gate or pressure at drain), p by a reference pressure, p_0, Eq.(9) is expressed in dimensionless terms as

$$\frac{Dh_0}{L^4}\frac{\partial^4 \hat{\delta}}{\partial \hat{x}^4} + h_0 cf\frac{\partial \hat{\delta}}{\partial \hat{t}} + \rho_m df^2 h_0 \frac{\partial^2 \hat{\delta}}{\partial \hat{t}^2}$$
$$= p_0(\hat{p} - \hat{p}_g) + \frac{Ed}{2(1-v^2)}\frac{h_0^3}{L^4}\left(\int_0^1 \left(\frac{\partial \hat{\delta}}{\partial \hat{x}}\right)^2 d\hat{x}\right)\frac{\partial^2 \hat{\delta}}{\partial \hat{x}^2} \tag{10}$$

where that hats denote dimensionless quantities. The deflection $\hat{\delta}(x,t)$ is then governed by

$$\frac{\partial^4 \hat{\delta}}{\partial \hat{x}^4} + \frac{cfL^4}{D}\frac{\partial \hat{\delta}}{\partial \hat{t}} + \frac{\rho_m df^2 L^4}{D}\frac{\partial^2 \hat{\delta}}{\partial \hat{t}^2}$$
$$= \frac{p_0 L^4}{Dh_0}(\hat{p} - \hat{p}_g) + 6\frac{h_0^2}{d^2}\left(\int_0^1 \left(\frac{\partial \hat{\delta}}{\partial \hat{x}}\right)^2 d\hat{x}\right)\frac{\partial^2 \hat{\delta}}{\partial \hat{x}^2} \tag{11}$$

Inertia and damping effects can be neglected when $\frac{\rho_m df^2 L^4}{D} << 1$ and $\frac{cfL^4}{D} << 1$ respectively. So if the forcing frequency f is much less than $\sqrt{\frac{D}{\rho_m dL^4}}$ and $\frac{D}{cL^4}$, the effects of inertia and damping can be neglected and the plate can be assumed to instantly

respond to pressure loading with quasi-static deflection deflection profile governed by

$$\frac{\partial^4\hat{\delta}}{\partial\hat{\mathbf{x}}^4} - 6\beta^2\left(\int_0^1\left(\frac{\partial\hat{\delta}}{\partial\hat{\mathbf{x}}}\right)^2 d\hat{\mathbf{x}}\right)\frac{\partial^2\hat{\delta}}{\partial\hat{\mathbf{x}}^2} = \Pi(\hat{\mathbf{p}} - \hat{\mathbf{p}}_g) \tag{12}$$

where $\beta \equiv h_0/d$ and $\Pi \equiv \frac{p_0 L^4}{Dh_0} = 12(1-v^2)\frac{\beta^3 p_0}{\alpha^4 E}$, and $\alpha = h_0/L$. It can be seen from Eq. (12) that for deflections much less than the plate thickness, pure bending dominates stretching, whereas stretching dominates pure bending when the deflection is larger than plate thickness. Note that although structural damping is neglected, the damping force imparted by the fluid on the plate dynamics is present through the coupling of the pressure distribution in the fluid with the viscous shear. The solution of Eq. (12) is

$$\hat{\delta}(\hat{\mathbf{x}},\hat{\mathbf{t}}) = C_1(\hat{\mathbf{t}})\sinh(a\hat{\mathbf{x}}) + C_2(\hat{\mathbf{t}})\cosh(a\hat{\mathbf{x}}) + C_3(\hat{\mathbf{t}})\hat{\mathbf{x}} + C_4(\hat{\mathbf{t}})g(\hat{\mathbf{x}}) + C_0(\hat{\mathbf{t}}) \tag{13}$$

where

$$
\begin{aligned}
C_1 &= \frac{g(1)a\sinh(a) + (1-\cosh(a))g'(1)}{a^2 B} \\
C_2 &= \frac{(1-\cosh(a))ag(1) + (-a+\sinh(a))g'(1)}{a^2 B} \\
C_3 &= \frac{-a^2 g(1)\sinh(a) + (\cosh(a)-1)ag'(1)}{a^2 B} \\
C_4 &= \frac{a^2\sinh(a) + 2(1-\cosh(a))a}{a^2 B} \\
C_0 &= \frac{(\cosh(a)-1)ag(1) + (a-\sinh(a))g'(1)}{a^2 B}
\end{aligned}
$$

$$
\begin{aligned}
B &= 4 + 2a\sinh(a) - 4\cosh(a) \\
g(\hat{\mathbf{x}},\hat{\mathbf{t}}) &= \int_0^{\hat{\mathbf{x}}}\int_0^{x_3}\left(e^{a(\hat{\mathbf{t}})x_2}\left(\int_0^{x_2} e^{-a(\hat{\mathbf{t}})x_1} f(x_1,\hat{\mathbf{t}})dx_1\right)\right. \\
&\quad\left. - e^{-a(\hat{\mathbf{t}})x_2}\left(\int_0^{x_2} e^{a(\hat{\mathbf{t}})x_1} f(x_1,\hat{\mathbf{t}})dx_1\right)\right)dx_2 dx_3
\end{aligned}
\tag{14}
$$

where $g' = dg/d\hat{\mathbf{x}}$, and $f(\hat{\mathbf{x}}, \hat{\mathbf{t}}) = \Pi(\hat{\mathbf{p}}(\hat{\mathbf{x}}, \hat{\mathbf{t}}) - \hat{\mathbf{p}}_g)$, and the parameter $a(\hat{\mathbf{t}}) = \sqrt{6\beta^2 \int_0^1 \left(\frac{\partial \hat{\delta}(\hat{\mathbf{x}}, \hat{\mathbf{t}})}{\partial \hat{\mathbf{x}}}\right)^2 d\hat{\mathbf{x}}}$, is the solution of the nonlinear equation

$$
\int_0^1 C_4 g'(\hat{\mathbf{x}}) \left(C_4 g'(\hat{\mathbf{x}}) + 2\left(C_1 a \cosh(a\hat{\mathbf{x}}) + C_2 a \sinh(a\hat{\mathbf{x}} + C_3)\right)\right) d\hat{\mathbf{x}}
$$

$$
+ C_3^2 + C_1 C_2 a \sinh(a)^2 + \frac{1}{2}(C_1^2 + C_2^2)a\cosh(a)\sinh(a)
$$

$$
- 2C_2 C_3 (1 - \cosh(a)) + 2C_1 C_3 \sinh(a) + \frac{1}{2}(C_1^2 - C_2^2)a^2 = \frac{a^2}{6\beta^2}
$$

Equation (13) constitutes the plate deflection model that yields the deflection for given gate pressure and flow pressure distribution along the channel.

B. Fluid Flow in the Channel

Coupling between the plate deformation and the fluid flow in the channel is through the pressure distribution in the flow, $\hat{\mathbf{p}}$, and the plate deflection, $\hat{\delta}$. In the fluid side, the conservation of mass and momentum for a Newtonian incompressible fluid are governed by the following equations

$$\nabla . \mathbf{u} = 0 \tag{15}$$

$$\rho_f \left(\frac{\partial \mathbf{u}}{\partial t} + \mathbf{u} . \nabla \mathbf{u} \right) = -\nabla p + \mu \nabla^2 \mathbf{u} \tag{16}$$

where $\mathbf{u}$ is the velocity vector, ρ_f and μ are respectively the density and dynamic viscosity of the fluid. The gravity body force is neglected, as is typical in microflows. For $h_0 << L$ and $h_0 << W$, the flow may be modeled as two-dimensional in the $x - y$ domain. Scaling t by $1/f$, x by L, y by h_0, p by a reference pressure drop along the channel, $p_{ds,0}$ so that $\frac{\partial p}{\partial x}$ scales as $\frac{p_{ds,0}}{L}$, and u by $U = \frac{h_0^2}{12\mu} \frac{p_{ds,0}}{L}$ (Note that $U = U_{pois}$, the average speed of a Poiseuille flow in a channel of height h_0 due to a reference pressure drop of $p_{ds,0}$), the component of the momentum equation (16) along the flow direction is expressed in dimensionless form as

$$\texttt{Re0} \left(\texttt{St0} \frac{\partial \hat{\mathbf{u}}}{\partial \hat{\mathbf{t}}} + \alpha\, \hat{\mathbf{u}} . \hat{\nabla} \hat{\mathbf{u}} \right) = -\texttt{Po} \frac{\partial \hat{\mathbf{p}}}{\partial \hat{\mathbf{x}}} + \frac{\partial^2 \hat{\mathbf{u}}}{\partial \hat{\mathbf{y}}^2} + \alpha^2 \frac{\partial^2 \hat{\mathbf{u}}}{\partial \hat{\mathbf{x}}^2} \tag{17}$$

where $\texttt{Re0} = \frac{U_{pois} h_0}{\nu_f}$, $\texttt{St0} = \frac{f h_0}{U_{pois}}$, and $\texttt{Po} = 12$ are respectively the Reynolds, Strouhal, and Poiseuille numbers. In what follows, we drop the hats and present flow model for the cases when the flow is inertia-free and when the flow has some inertia.

1. The Inertia-free Channel Flow Model

When inertia effects are negligible ($\text{Re0} << 1$ and $\text{Re0.St0} << 1$) or when the flow is steady ($\partial u/\partial t = 0$) and nearly parallel $\alpha << 1$, the momentum equation in the flow direction may be approximated as

$$0 \simeq -\text{Po}\frac{\partial p}{\partial x} + \frac{\partial^2 u}{\partial y^2} \tag{18}$$

Since from continuity (15), $v \sim \alpha u$, it can be seen by comparing the x and y component of the momentum equation that $\left|\frac{\partial p/\partial y}{\partial p/\partial x}\right| \sim \alpha$, so that for $\alpha << 1$, $p \simeq p(x,t)$. Integrating Eq.(18), subject to no-slip boundary conditions $u(0) = u(h) = 0$, we get

$$u_0 = \frac{\eta(1-\eta)h^2\text{Po}}{2}\left(-\frac{\partial p}{\partial x}\right) \tag{19}$$

where $\eta \equiv y/h(x)$ and the subscript 0 denotes inertia-free solution. Expressing $h(x,t) = 1 + \delta(x,t)$, the volume flow-rate (normalized by Uh_0) is then

$$Q_0 = (1+\delta)^3\left(-\frac{\partial p}{\partial x}\right) \tag{20}$$

Noting that, from conservation of mass, Q does not vary in x, the flow rate and the pressure distribution along the channel are given by

$$Q_0 = p_{ds}\left(\int_0^1 \frac{1}{(1+\delta)^3}dx\right)^{-1} \tag{21}$$

and

$$p_0 = p_d - Q_0\int_0^x \frac{1}{(1+\delta(\chi,t))^3}d\chi \tag{22}$$

where p_{ds} is the pressure drop along the channel. Equations (21) and (22) constitute the inertia-free model of the channel flow that yields the pressure distribution along the channel and the volume flow-rate for a given plate deflection profile $\delta(x)$.

2. The Low Inertia Channel Flow Model

To account for inertia, the inertia term is estimated from the velocity solution of the inertia-free model, and the pressure distribution and the flow rate are then updated. The continuity equation is used to get an expression for v, with u_0 and p_0, so that

$$v_1 = \frac{\text{Po}}{2A(1)} \frac{h'}{h} \eta^2 (1 - \eta) p_{ds}$$

where $h' = dh/dx$, $A(x) = \int_0^x dx'/h(x')^3$ and the subscript 1 refers to solution with inertia correction. Note that, from the continuity equation, v is scaled by αU_{pois}. An improved estimate of the pressure can then be obtained from the $y-$component of the momentum equation, where we assume that the pressure term balances the diffusion term (negligible inertia)

$$0 \simeq -\text{Po} \frac{\partial p_1}{\partial y} + \alpha^2 \frac{\partial^2 v_1}{\partial y^2}$$

which yields

$$p_1 \simeq \frac{\alpha^2 p_{ds}}{A(1)} \frac{h'}{h^2} \left(\eta - \frac{3}{2} \eta^2 \right) + f(x) \tag{23}$$

where $f(x) = p_1(x, y = 0)$ is the pressure distribution at the lower wall. Note also that $p_d = \int_0^1 p_1(0, y) dy$ and $p_s = \int_0^1 p_1(1, y) dy$. An improved solution of u that includes correction for inertia is determined by solving the steady momentum equation in the flow direction

$$\alpha \text{Re} \left(u_0 \frac{\partial u_0}{\partial x} + v_1 \frac{\partial u_0}{\partial y} \right) = -\text{Po} \frac{\partial p_1}{\partial x} + \frac{\partial u_1^2}{\partial y^2} \tag{24}$$

The solution of Eq. (24), upon satisfying the no-slip boundary conditions at solid walls, is

$$
\begin{aligned}
u_1 &= \frac{\alpha \text{Re} \text{Po}^2}{240 A(1)^2} \frac{h'}{h} \left(\eta - 5\eta^4 + 6\eta^5 - 2\eta^6 \right) p_{ds}^2 + \frac{\text{Po}}{2} h^2 f' \eta (\eta - 1) \\
&+ \frac{\alpha^2 \text{Po}}{2A(1)} \left(\left(\frac{h'^2}{h} - \frac{h''}{4} \right) \eta^4 - \left(\frac{h'^2}{h} - \frac{h''}{3} \right) \eta^3 - \frac{h''}{12} \eta \right) p_{ds}
\end{aligned} \tag{25}
$$

17

where $f' \equiv df/dx$. Noting that $f(0) = p_d$ and $f(1) = p_s$, equation (25) is integrated to get the flow rate as

$$Q_1 = Q_0 \left[1 - \frac{\alpha^2}{10A(1)} \int_0^1 \left(\frac{3h'^2}{h^3} + \frac{h''}{2h^2} - \frac{9}{7} \frac{\mathrm{Re}Q_0}{\alpha} \frac{h'}{h^3} \right) dx \right] \qquad (26)$$

The function $f(x)$ can be determined by noting that $Q_1 = \int_0^{h(x)} u_1 dy$ is independent of x, resulting in the pressure distribution

$$
\begin{aligned}
p_1 \quad \simeq \quad & p_0 + \alpha^2 Q_0 \left\{ \frac{h'}{h^2} \left(\eta - \frac{3}{2}\eta^2 \right) - \frac{1}{10} \int_0^x \left(\frac{3h'^2}{h^3} + \frac{h''}{2h^2} - \frac{9}{7} \frac{\mathrm{Re}Q_0}{\alpha} \frac{h'}{h^3} \right) dx' \right. \\
& + \left. \frac{1}{10} \frac{A(x)}{A(1)} \int_0^1 \left(\frac{3h'^2}{h^3} + \frac{h''}{2h^2} - \frac{9}{7} \frac{\mathrm{Re}Q_0}{\alpha} \frac{h'}{h^3} \right) dx \right\}
\end{aligned}
\qquad (27)
$$

Equations (26) and (27) constitute the low inertia model of the channel flow that yields the pressure distribution along the channel and the volume flow-rate for a given plate deflection profile $\delta(x)$.

C. DC Operating Point

The low-inertia model exhibits a nonlinear dependence of the flowrate (current) on the drain-source and gate-source pressure differences $\hat{\mathbf{p}}_{ds}$ and $\hat{\mathbf{p}}_{gs}$. The flowrate also depends on Reynolds number of the flow, $\mathtt{Re}$, the structural parameter, Π, and the aspect ratio, α.

$$\hat{\mathbf{Q}} = \hat{\mathbf{Q}}(\hat{\mathbf{p}}_{ds}, \hat{\mathbf{p}}_{sg}, \mathtt{Re}, \alpha, \Pi) \tag{28}$$

where $\hat{\mathbf{p}}_{sg} = -\hat{\mathbf{p}}_{gs}$ is the source-gate pressure difference. For a given device geometry, material properties, and reference pressure $\hat{\mathbf{p}}_{ds,0}$, the dimensionless parameters $\mathtt{Re}$, Π, and α are constant and the flow rate is a function of both $\hat{\mathbf{p}}_{sg}$ and $\hat{\mathbf{p}}_{ds}$

$$\hat{\mathbf{Q}} = \hat{\mathbf{Q}}(\hat{\mathbf{p}}_{ds}, \hat{\mathbf{p}}_{sg}) \tag{29}$$

It should be noted that in some cases there are two equilibrium values of $\hat{\mathbf{Q}}$ for a given $\hat{\mathbf{p}}_{ds}$ and a given $\hat{\mathbf{p}}_{sg}$. As will be shown in section IV, these two operating points are characterized by different deflection profiles of the plate, different pressure distribution along the channel, and different values of Reynolds number indicating that the channel flow in one of these two operating points has higher inertia.

In static (steady) conditions, the device operates as a variable resistance controlled by the gate pressure, with the resistance given as

$$\hat{\mathbf{R}}(\hat{\mathbf{p}}_{ds}, \hat{\mathbf{p}}_{sg}) = \frac{\hat{\mathbf{p}}_{ds}}{\hat{\mathbf{Q}}} \tag{30}$$

On the other hand the dynamic behavior of the device is divided into two portions. The capacitve part where the deflection of the membrane is upwards and the transistive part where its downward. These two parts are discussed next .

D. Capacitance

The capacitive behavior of the device can be investigated through the dependence of the mass stored in the device on gate-drain and source-gate pressure difference. The stored mass is

$$\hat{\mathbf{m}}(\hat{\mathbf{t}}) = \int_0^1 (1 + \hat{\delta}(\hat{\mathbf{x}}, t)) d\hat{\mathbf{x}} = \hat{\mathbf{m}}(\hat{\mathbf{p}}_{ds}(\hat{\mathbf{t}}), \hat{\mathbf{p}}_{sg}(\hat{\mathbf{t}})) \tag{31}$$

where $\hat{\mathbf{m}} = m/(\rho W L h_0)$, then

$$\frac{d\hat{\mathbf{m}}(\hat{\mathbf{t}})}{\partial \hat{\mathbf{t}}} = \hat{\mathbf{C}}_{ds}\frac{d\hat{\mathbf{p}}_{ds}}{d\hat{\mathbf{t}}} + \hat{\mathbf{C}}_{sg}\frac{d\hat{\mathbf{p}}_{sg}}{d\hat{\mathbf{t}}} \tag{32}$$

where respectively

$$\hat{\mathbf{C}}_{ds} \equiv \frac{\partial \hat{\mathbf{m}}}{\partial \hat{\mathbf{p}}_{ds}} \tag{33}$$

$$\hat{\mathbf{C}}_{sg} \equiv \frac{\partial \hat{\mathbf{m}}}{\partial \hat{\mathbf{p}}_{sg}} \tag{34}$$

$\hat{\mathbf{C}}_{ds}$ is the drain-source capacitance; the increase in the mass stored per unit increase in drain-source pressure difference while holding the source-gate pressure difference constant. Similarly, $\hat{\mathbf{C}}_{sg}$ is the source-gate capacitance measuring the increase in the mass stored per unit increase in the source-gate pressure difference while holding the drain-source pressure difference constant. As will be shown in section IV, there exist an operation region where a negative C_{ds} capacitance is observed, indicating a reduction in the mass stored as the drain-source pressure difference is increased, for a given source-gate pressure difference. The negative capacitance can be attributed to the significant role of inertia in that region of operation.

20

E. Small Signal Behavior (Model)

Small signal operation of the device is similar to that of an electronic transistor where the flowrate (current) is controlled by the pressure difference between the drain and the source (drain-source voltage) and the pressure difference between the gate and the source (gate-source voltage). At small frequencies, inertia effects can be neglected, and the device behaves as pressure (voltage) controlled volume flowrate (current) source. The model presented in the previous section exhibits a nonlinear dependence of the flowrate (current) on the normalized drain-source and source-gate pressure differences $\hat{\mathbf{p}}_{ds}$ and $\hat{\mathbf{p}}_{sg}$. Small signal models, that assume that the pressure signals experiences a small time-varying (AC) component on top of a DC Operating Point (or Bias), are commonly used to carry out fast small signal analysis of complex electronic circuits. Expressing the source-gate pressure difference, drain-source pressure difference and the volume flowrate as the sum of a steady operating point (DC) component and a small time-varying component,

$$p_{sg}(t) = p_{sg,DC} + p'_{sg}(t)$$

$$p_{ds}(t) = p_{ds,DC} + p'_{ds}(t)$$

$$Q(t) = Q_{DC} + Q'(t) \tag{35}$$

where $|p'_{sg}/p_{sg,DC}| << 1$, $|p'_{ds}/p_{ds,DC}| << 1$, and $|A'/Q_{DC}| << 1$. For a given device geometry, material properties, and reference pressure $p_{ds,0}$, the dimensionless parameters Re, Π, and α are constant and the flow rate is a function of both p_{sg} and p_{ds}

$$dQ = \left.\frac{\partial Q}{\partial p_{ds}}\right|_{p_{sg}} dp_{ds} + \left.\frac{\partial Q}{\partial p_{sg}}\right|_{p_{ds}} dp_{sg} \tag{36}$$

It can then be shown that a linear relationship among the small signal components is obtained as

$$Q'(t) \simeq g_m p'_{sg}(t) + \frac{1}{r_o} p'_{ds}(t) \tag{37}$$

The small signal behavior is expressed in Eq. (37) in a manner that is analogous to that of electronic MOSFET, where g_m and r_o are respectively the transconductance and intrinsic output resistance

$$g_m = \left. \frac{\partial Q}{\partial p_{sg}} \right|_{p_{ds,DC}} \tag{38}$$

$$r_o = \left(\frac{\partial Q}{\partial p_{ds}} \right)^{-1}_{p_{sg,DC}} \tag{39}$$

In dimensionless form,

$$g_m = \frac{Wh_0^3}{12\mu L} \left(\frac{\partial \hat{\mathbf{Q}}}{\partial \hat{\mathbf{p}}_{sg}} \right) = \frac{Wh_0^3}{12\mu L} \hat{\mathbf{g}}_m \tag{40}$$

$$r_o = \frac{12\mu L}{Wh_0^3} \left(\frac{\partial \hat{\mathbf{Q}}}{\partial \hat{\mathbf{p}}_{ds}} \right)^{-1} = \frac{12\mu L}{Wh_0^3} \hat{\mathbf{r}}_o \tag{41}$$

The intrinsic small signal gain in the pressure, defined as $A_v = p'_{ds}/p'_{sg}$, is given by the product

$$A_v = \hat{\mathbf{g}}_m \hat{\mathbf{r}}_o \tag{42}$$

The intrinsic gain is the maximum gain that can be achieved using a single transistor. The small signal model of the low-inertia behavior is described by the circuit shown in Fig. 4. The models corresponds to a pressure (voltage) controlled flowrate (current) source in parallel with intrinsic output resistance r_o. The source-gate and drain-source

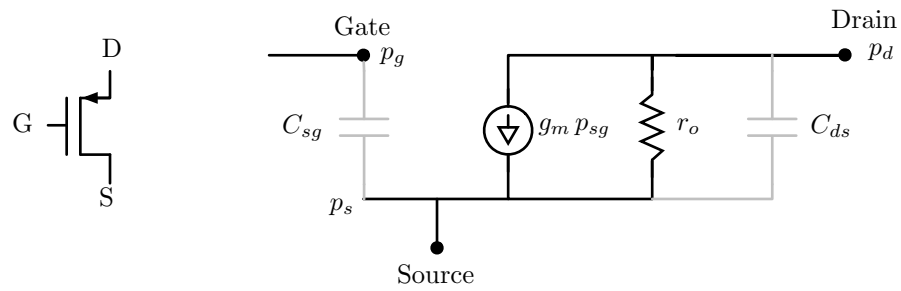capacitances are also shown in the circuit.

Figure 4: Low frequency small signal microfluidic transistor model.

Numerical implementation of the model, along with determination of the capacitances and the small signal parameters, is discussed in the following section. Discussion of the different operation regimes, based on the detailed computational solution of the fluid-structure interaction problem is presented in section IV.

CHAPTER III

MODEL IMPLEMENTATION

The model presented in the previous section enables fast computation of the membrane deflection (Eq. (13)) and fluid flow rate (Eq. (20) or (26)) and pressure distribution (Eq. (22) or (27)) using the following simple iterative method. The method starts by assuming an initial linear pressure profile similar to that in a poiseuille flow,

$$\hat{\mathbf{p}}(x) = -\hat{\mathbf{p}}_{ds}\hat{\mathbf{x}} + \hat{\mathbf{p}}_d. \tag{43}$$

The pressure is then plugged in Eq.(13) to get a deflection profile $\hat{\delta}(x)$ of the membrane. The deflection profile is then inserted in the flow rate equations Eq.(20) and Eq.(26) to determine the inertia free flow Q_0 and inertia flow rate Q_1 respectively. The flow rate is then used in Eq.(22) and Eq.(27) to update the pressure profile of the flow under the membrane. This process, illustrated in Fig. 5, is repeated until the solution is converged.

The capacitances and the small signal parameters (transconductance and intrinsic resistance) are determined by numerically discretizing the derivatives in Eqs. (33), (34), (38) and (39) using the procedure of Fig. 5 to find the solution at the discretization points.
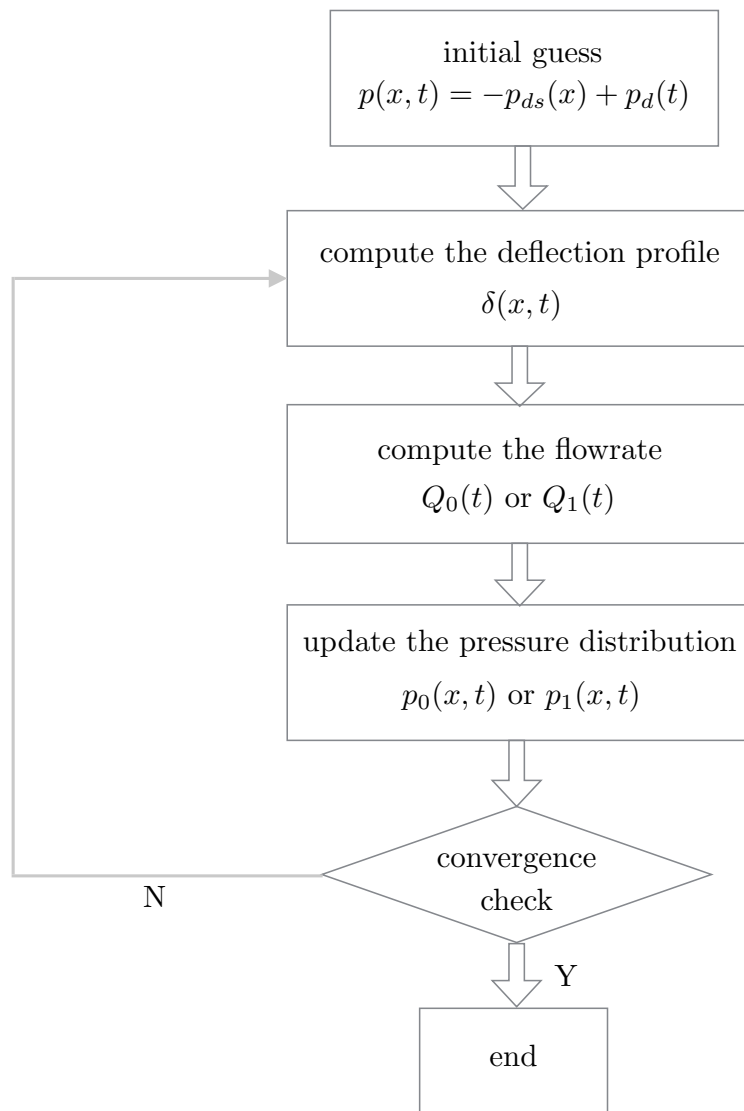
Figure 5: Flow chart of model implementation.

CHAPTER IV

OPERATION REGIONS

In this section, we present the static behavior of the 2D pressure-actuated microfluidic transistor depicted in Fig. 3, using FSI (Fluid Structure Interaction) simulations on FLUENT/ANSYS over ranges of operating pressures ($p_{ds} = p_d - p_s$ and $p_{gs} = p_s - p_g$). This behavior is presented as characteristic curves similar to those relating the drain current to drain-source and gate-source voltage differences in a MOSFET. These characteristic curves are then used as the basis for choosing the "DC" operating point (bias) of the transistor and extraction of the capacitances and the small signal parameters such as transconductance, intrinsic output resistance, and pressure gain. The large signal steady (DC) behavior as well as the small signal unsteady (AC) behavior will be compared and contrasted with those of a standard MOSFET.

As depicted in Fig. 3, the membrane is fixed from both sides ($x = 0$ and $x = L$). In our simulations, the length of the membrane is $L = 3118\mu$m, the (undeformed) channel height is $h_0 = 59\mu$m, the depth is $L_z = 500\mu$m, and the membrane thickness is $d = 196\mu$m. These dimensions are similar to those used for the fluidic capacitor presented in [11]. The numerical results are obtained from ANSYS numerical simulations of the coupled fluid-structure interaction. At each time step, the FLUENT solution of the pressure distribution in the fluid is used by ANSYS to solve for the deflection of the membrane, which in then used to update the mesh in FLUENT for the following time step, and so on. Although the simulation is performed using a 3D setup, the depth is discretized using a single computational element with symmetry imposed on either side. So the problem considered is essentially two-dimensional with plane strain conditions imposed for the plate. Comparison with the more realistic 3D cases is presented in section V. The mesh is made of cubic elements having a maximum size of

$10\,\mu$m. The mesh size is chosen so that the solution is nearly mesh-independent. In addition, the mesh is dynamic and changes size as the solid and the fluid domains deform To ensure a fully developed flow at the inlet of the transistor, an entry section is added at the drain side of the transistor with a length of $L_e = 600\mu$ and height $h_e = h_0 = 59\,\mu$m. This entry length is chosen large enough for the flow to reach fully developed conditions at the drain while at the same time much shorter than the transistor length so that it introduces a resistance to the flow much smaller than that of the transistor itself. The boundary conditions at the entry section is prescribed in terms of a velocity inlet and assumed to be uniform. At the outlet of the transistor atmospheric pressure is prescribed, i.e. $p_s = p_{atm}$. A uniform gate pressure, p_g, is imposed as boundary conditions in the structure part of the numerical solver.

A. Operating Point (DC) Characteristic Curves

At static (steady) operation, the device behaves as variable resistor controlled by the gate-source pressure difference, with the resistance given by Eq. (30). As can be observed from Fig. 6, the resistance increases with the gate-source pressure difference, at a given drain-source pressure difference. This is because increasing the gate-drain pressure difference causes a downward deflection of the plate thus reducing the channel height, which significantly increases the resistance. For a poiseuille flow, the resistance behaves as $R \sim h^{-3}$. It can also be observed from Fig. 6 that increasing the drain-resistance pressure difference, while keeping the gate-source pressure difference constant, decreases the resistance. This is again attributed to the upward deflection caused by increasing the pressure in the channel.

Following the procedure conventionally used in small signal characterization of electronic transistors [17], we present in Fig. 7 a plot of the volume flow rate $\hat{\mathbf{Q}}$ versus $\hat{\mathbf{p}}_{ds}$ for fixed values of $\hat{\mathbf{p}}_{gs}$. The corresponding plate deflection, presented in terms of the normalized maximum and/or minimum deflections, is plotted in Fig. 8. By inspecting these figures, the following regions of operation are identified based on the deflection of the plate: (i) positive capacitance regime (upward plate deflection), (ii) negative capacitance regime (upward plate deflection with significant inertia role), and (iii) a transistor region (downward plate deflection).
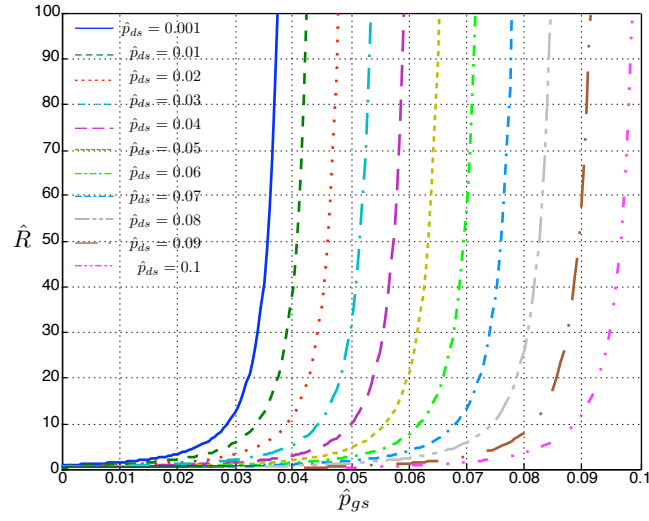
(a) $\hat{\mathbf{R}}$ - $\hat{\mathbf{p}}_{gs}$
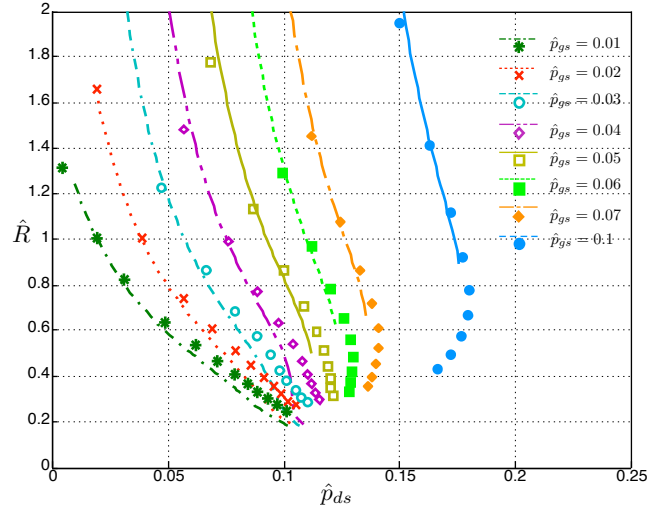
(b) $\hat{\mathbf{R}}$ - $\hat{\mathbf{p}}_{ds}$

Figure 6: Static Resistance $\hat{\mathbf{R}}$ for different operating pressures

B. Capacitive Region

The capacitance region is characterized by upward deflection of the membrane which occurs when p_{ds} is sufficiently larger that p_{gs}, or when $p_{ds} > p_{ds}^*$. Increasing the drain-source pressure difference, for a given gate drain pressure difference, causes the plate to deflect further upwards, so that more mass is stored and the drain-source capacitance is positive; $\hat{\mathbf{C}}_{ds} > 0$. The dependence of drain-source and gate-source capacitances versus gate-source pressure difference is presented in Fig. 9 for different
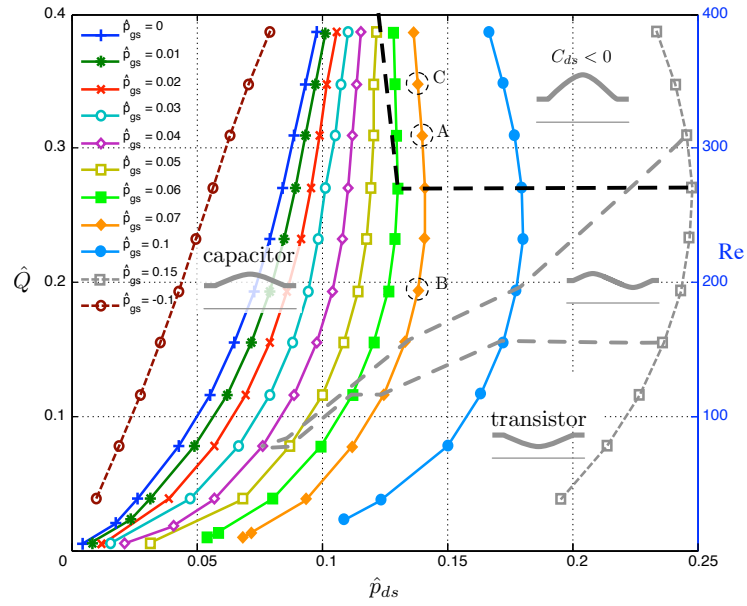
Figure 7: $\hat{\mathbf{Q}} - \hat{\mathbf{p}}_{ds}$ Characteristics of the mirofluidic transistor.

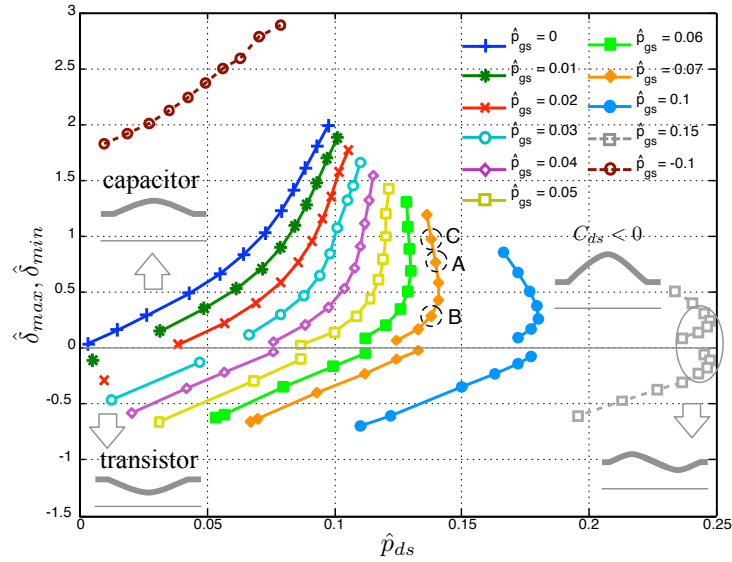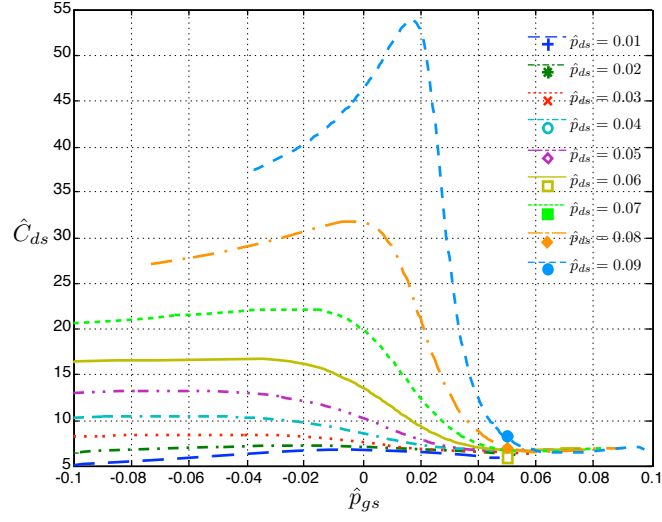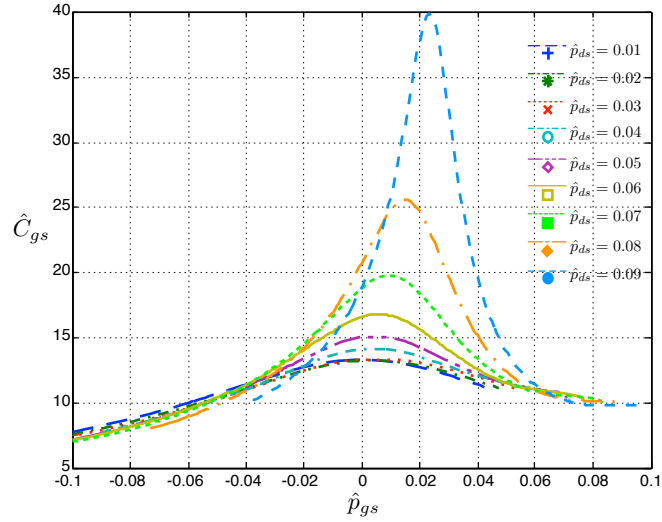Figure 8: Plate maximum and/or minimum deflection. Positive indicated upwards deflection, negative indicates downward deflection.

values of p_{ds}.

(a) $\hat{\mathbf{C}}_{ds} - \hat{\mathbf{p}}_{gs}$

(b) $\hat{\mathbf{C}}_{gs} - \hat{\mathbf{p}}_{ds}$

Figure 9: Drain-Source and Gate-Source Capacitance for fixed values of $\hat{\mathbf{p}}_{ds}$

The characteristic drain-source pressure difference, p_{ds}^*, above which the device enters the negative capacitive region exhibits a linear dependence on the gate-source presure difference, as depicted in Fig. 10.

In the capacitive region, it is observed in some cases, that for given drain-source and gate-source pressure differences, there exist two separate operating points, such as points A and B in Fig. 7. Point A is characterized by a larger flow rate (large Re) and
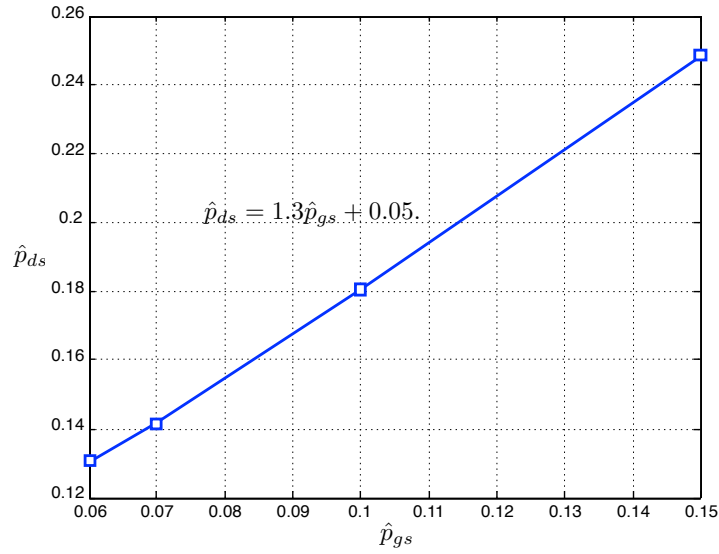
Figure 10: Minimum drain-source pressure separating the negative capacitive behavior from the capacitive and transistive behavior.

larger upward deflection than point B. As can be observed from Fig. 11. The large deflection at point B is in part, sustained by a larger pressure in the channel caused by expansion of the flow in the larger channel. In effect, the large upward deflection and the corresponding pressure recovery in the channel enhance one another. Point A belongs to a negative drain-source capacitance region. This can be illustrated by inspecting points A and C in Fig. 8. While both points have the same gate-source pressure differece, point C is characterized by a larger upwards deflection and a smaller drain-source pressure difference when compared to point A, which implies that more mass is stored as the operating point moved from A to C while the drain-source pressure difference has decreased, indicating that the drain-source capacitance is negative.
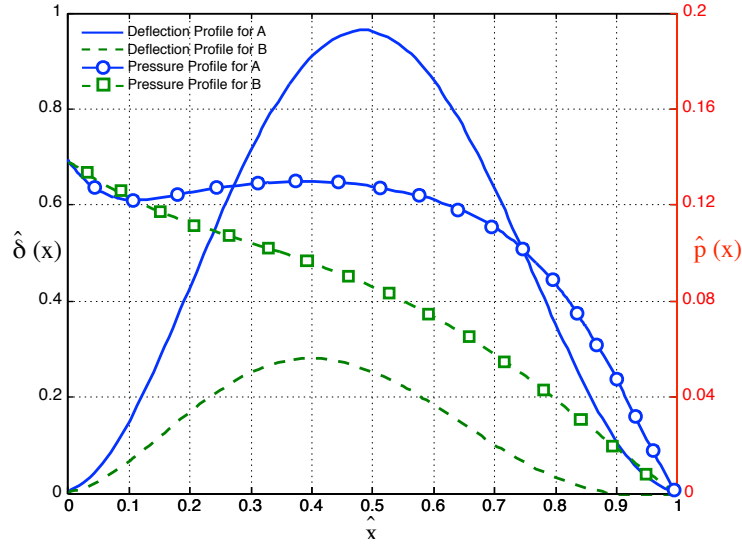
Figure 11: Deflection and pressure profile for points A and B

C. Transistive Region

When the plate deflection is downward or when it assumes an S shape, where it is upwards on the drain side and downward on the source side, the device behaves as a transistor that is capable of amplifying small signal gate-source pressure oscillations, p'_{gs}, to yield a small signal drain-source pressure difference, $p'_{ds} = A_v p'_{gs}$, where A_v is the pressure gain. There is, however, significant differences between this device and a electronic transistor. The MOSFET transitions from the ohmic region ($V_{ds} < Vgs - V_{th}$), where the small signal output resistance is finite and is equal to the DC resistance, to the saturation region ($V_{ds} > Vgs - V_{th}$) characterized by ideally an infinite incremental resistance r_o. In contrast, the small signal output resistance of the presented microfluidic transistor decreases as p_{ds} increases, which limits the gain, as will be illustrated shortly. As such, there is no distinction between a linear and saturation region, as can be deduced from Fig. **??**, where the DC ressitance and the small signal output ressitance are plotted against the drain-source pressure difference for a gate-source pressure difference of 0.05. Both the DC resistance and the small signal output resistance decrease as the drain-source pressure increases for positive values of the gate-drain pressure.
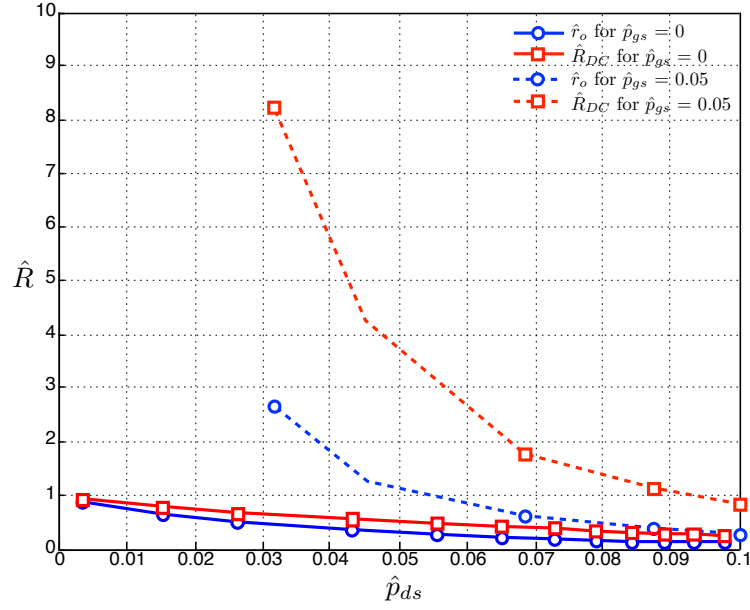
33

Figure 12: Variation of DC Resistance and AC output resistance versus drain-source pressure difference

For a given positive gate-source pressure difference the minimum drain-source pressure required to open the channel and have a finite flowrate depends to a large degree on the dimensionless parameters Π and β. For $p_{ds} < p_{gs}$, the plate deflection could be all the down so that the channel is closed if the plate is still in the bending regime and if its stiffness is not sufficiently large. If the plate is thinner than the channel, then stretching tends to prevent the channel from closing which results in a smaller minimum drain-source pressure difference required to open the channel.

Small Signal Parameters

In order to further enhance the characterization of the microfluidic transistor, further simulations are performed to compute the small signal parameters of the reduced order model. The new simulations generate plots for the intrinsic resistance and the transconductance for a set of $\hat{\mathbf{p}}_{gs}$ and $\hat{\mathbf{p}}_{ds}$ thus allowing us to produce other plots that combine the two of them. From Eq. (39), the intrinsic output resistance $\hat{\mathbf{r}}_o$, is obtained

by perturbing the drain pressure p_d (through perturbing the inlet velocity) and fixing all other parameters. It can be seen from Fig. 13 that the intrinsic resistance ($\hat{\mathbf{r}}_o$) decreases linearly with the increase of $\hat{\mathbf{p}}_{ds}$, until it reaches a minimum.
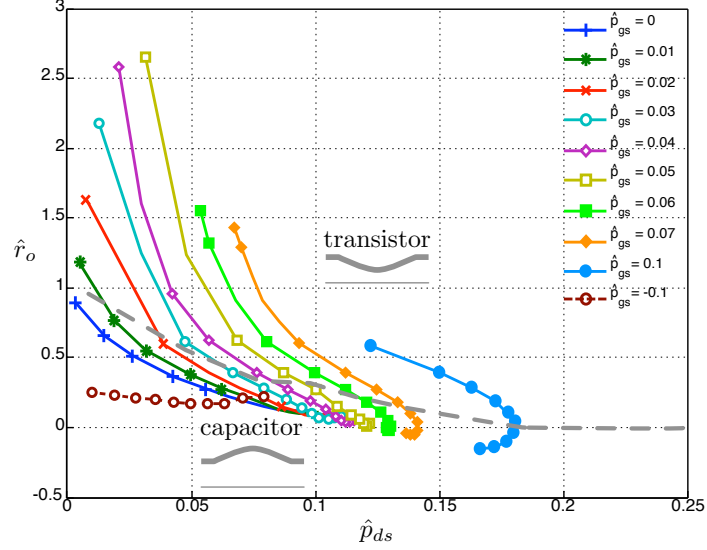

Figure 13: Intrinsic Resistance of microfluidic transistor for fixed $\hat{\mathbf{p}}_{gs}$.

The fluidic transconductance $\hat{\mathbf{g}}_m$ on the other hand can be obtained by fixing all parameters and applying a small signal perturbation to the external pressure $\hat{\mathbf{p}}_g$. Since the drain pressure $\hat{\mathbf{p}}_d$ can't be fixed due to the boundary conditions, then $\hat{\mathbf{g}}_m$ is obtained by using the intrinsic resistance calculated before as shown in equation below Eq. (38)

$$g_m = \frac{\partial \hat{\mathbf{Q}}}{\partial \hat{\mathbf{p}}_{gs}} = \frac{1}{r_o} \frac{\partial \hat{\mathbf{p}}_{ds}}{\partial \hat{\mathbf{p}}_{gs}} \tag{44}$$

It can be seen from Fig.14 and Fig.13 that $\hat{\mathbf{g}}_m$ and $\hat{\mathbf{r}}_o$ are inversely proportional where the minimum attained by $\hat{\mathbf{r}}_o$ for a given $\hat{\mathbf{p}}_{gs}$ corresponds to a maximum by $\hat{\mathbf{g}}_m$ for the same $\hat{\mathbf{p}}_{ds}$.

After running the simulations for calculating the intrinsic resistance and the transconductance, the gain can be calculated using Eq. (42) as shown in Fig. 15. One can see that the the gain A_v attains its peak values for small values of $\hat{\mathbf{p}}_{ds}$, where the
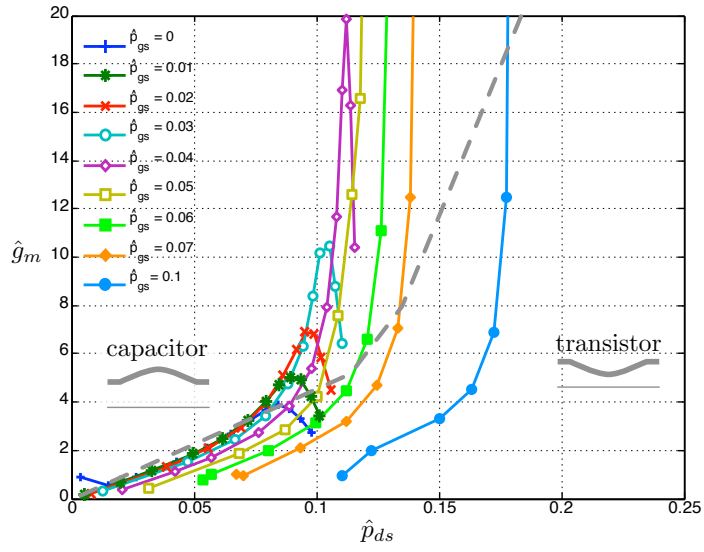
35

Figure 14: Fluidic Transconductance for fixed $\hat{\mathbf{p}}_{gs}$

membrane is deflected downward, and as $\hat{\mathbf{p}}_{ds}$ increases the membrane starts to bulge upward and the gain starts to decrease. It may be of interest to operate at the points of maximum gain to maximize the small signal component of the flowrate for an applied pressure difference.
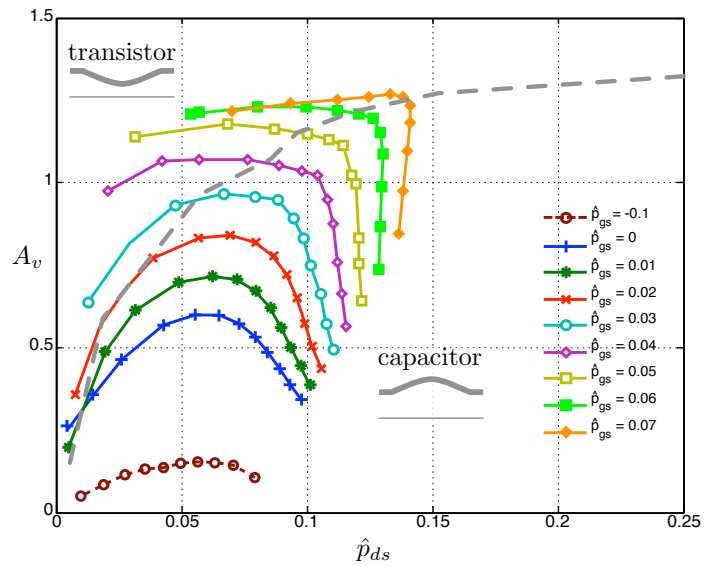

Figure 15: The Variation of the Gain with respect to $\hat{\mathbf{p}}_{gs}$ for $h_0 = 59\mu m$

The trend for the gain A_v differs completely when h_0 is increased from $59\mu m$ to

$250\mu m$ as shown in Fig.16, where instead of the gain dropping as $\hat{\mathbf{p}}_{ds}$ increases as the case with $h_0 = 59\mu m$, it keeps on increasing. In this case the maximum membrane deflection with respect to the channel height (δ_{max}/h_0) isn't affected by the pressure under the membrane $\hat{\mathbf{p}}_{ds}$, the same as the transistor with $h_0 = 59\mu m$. This implies that the membrane deflection plays a small role in controlling the gain and the gain is mainly regulated by the inertia of the flow, which is proportional to the pressure across the channel of the transistor $\hat{\mathbf{p}}_{ds}$.

From these results one can see that attaining high gains differs according to the type of transistor used. For transistors with thickness to gap ratio (d/h_0) greater than 1, the best method is to bulge the membrane down until δ/h_0 becomes very close to 1 as shown in Fig.15. As for transistors with channel height h_0 greater than the membrane d, the gain in these transistors is mainly controlled by the inertia of the flow high and thus the best method to attain high gains is to increase the pressure across the channel as shown in Fig. 16.
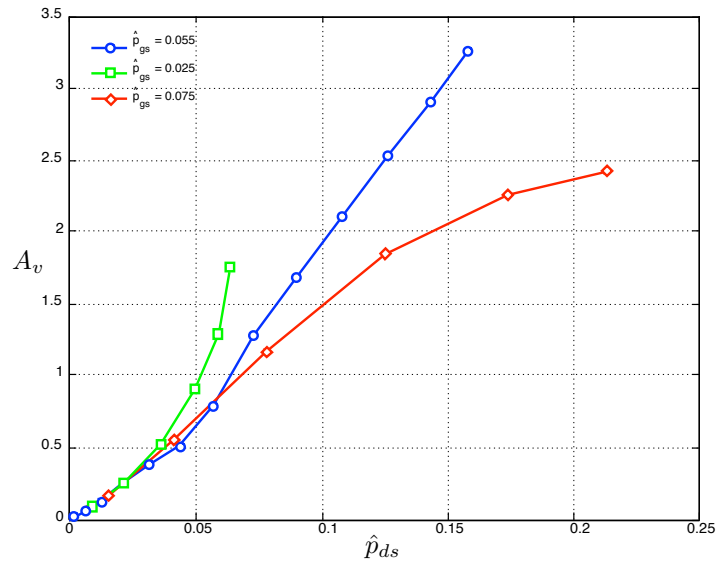

Figure 16: The Variation of the Gain with respect to $\hat{\mathbf{p}}_{gs}$ for $h_0 = 250\mu m$

CHAPTER V

MODEL VALIDATION

A. 3D Gain to 2D

The gain shown in the previous section was derived from a 2D simulation of the microfluidic transistor by using several assumptions to neglect 3D effects on the fluid and solid. These assumptions state that all the stress on the membrane in the z-component can be neglected, and any effect of the walls on the flow can be disregarded, thus allowing the device to be governed with 2D parameters only. In this section we investigate for what values of W/L can the 2D assumption be considered true. In order to simulate the 3D problem, we kept all boundary conditions of the 2D simulation the same except for the symmetry condition on the membrane and flow, which where replaced by fixed support for the membrane and no-slip walls for the flow. As for the mesh it became discretised in the z-direction. The results of the 3D simulation are plotted on Fig.17 in comparison to the 2D. From the figure one can see that for small values of W/L the 3D gain is much lower than the gain attained from the 2D case, due to the effect of the no slip conditions of the walls on the flow, and the additional fixed support on the deflection of the membrane. As W increases the influence done by the additional walls on the flow decreases, and the 3D gain starts to converge to become similar to the 2D gain.
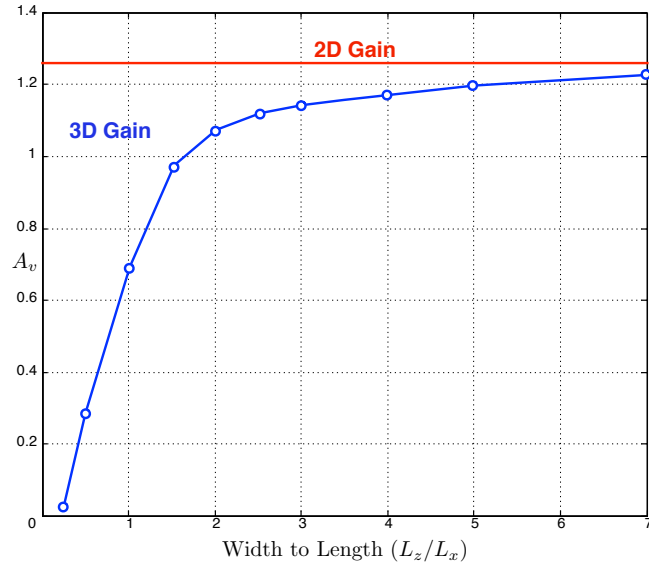
Figure 17: Convergence of the 3D Gain to the 2D Gain

B. Comparing Analytical Model to Numerical Results

The reduced order model parameters computed from ANSYS simulations in the previous section are compared with those predicted by the simplified models. The flow rate predicted by the model is shown along those computed from ANSYS simulations in Fig.18 , for fixed $\hat{\mathbf{p}}_{gs}$. It can be observed from Fig. 18 that the model yields more accurate results at small values of $\hat{\mathbf{p}}_{ds}$ for a given $\hat{\mathbf{p}}_{ds}$, as inferred by the agreement with the CFD solution. This is expected because the model is developed for low- inertia flows.

Gain computed by the CFD simulation is compared to those computed by the model in Fig. 19 for different values of $\hat{\mathbf{p}}_{gs}$. It can be observed that the model and the CFD simulation are close for small values of $\hat{\mathbf{p}}_{ds}$ and diverge as $\hat{\mathbf{p}}_{ds}$ increases. This is expected since, the gain Av is computed form the small signal parameters r_o and g_m, and each one of them is derived from $\hat{\mathbf{Q}}$, so since the flowrate obtained from the model diverges from CFD simulation as $\hat{\mathbf{p}}_{ds}$ increases as shown in Fig. 18, this divergence is multiplied when the gain Av is computed.
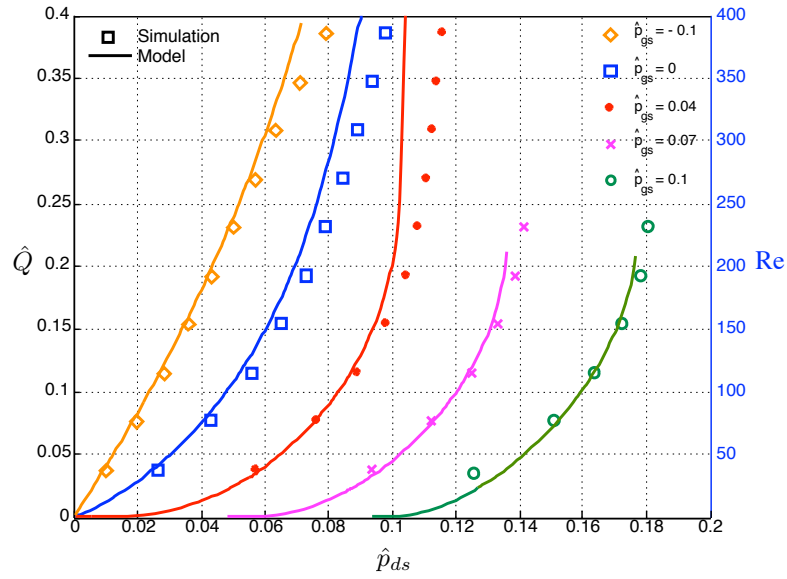
Figure 18: Comparison of the steady state flowrate $\hat{\mathbf{Q}}$ between the CFD simulation (Markers) and model (Line)
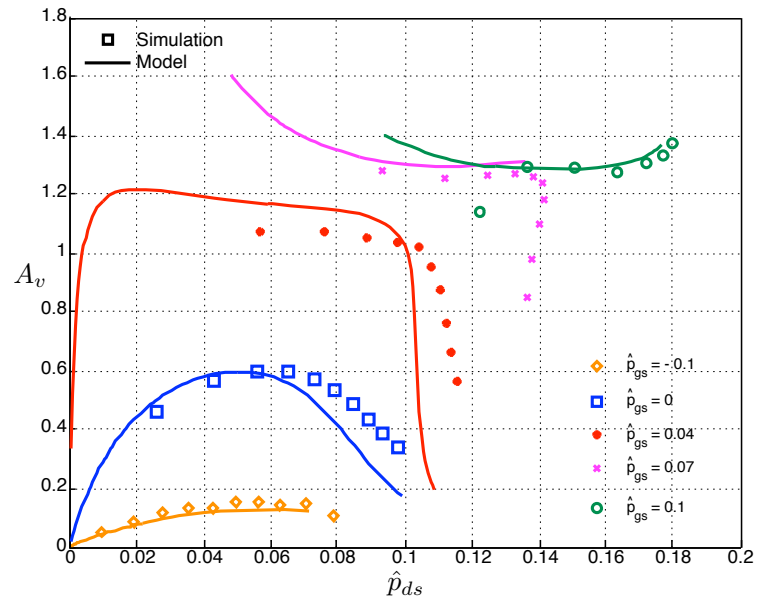

Figure 19: Comparison of the gain *Av* of the CFD simulation and model

In the last set of cases we compare the inertia free model, and the inertia model to the simulation. In this set of simulations the height of the channel is increased from $59\mu m$ to $250\mu m$, while all other geometric parameters are kept fixed. This is done to increase the effect of inertia on the flow, since Reynolds number is proportonal to h_0. The results are plotted in Fig. 20, it can be shown for small values of $\hat{\mathbf{p}}_{ds}$ the simulation and the models match, however as $\hat{\mathbf{p}}_{ds}$ increases the effect of inertia on the flow starts to grow and the free inertia model starts to diverge from the simulation results in contrary to the inertia model.
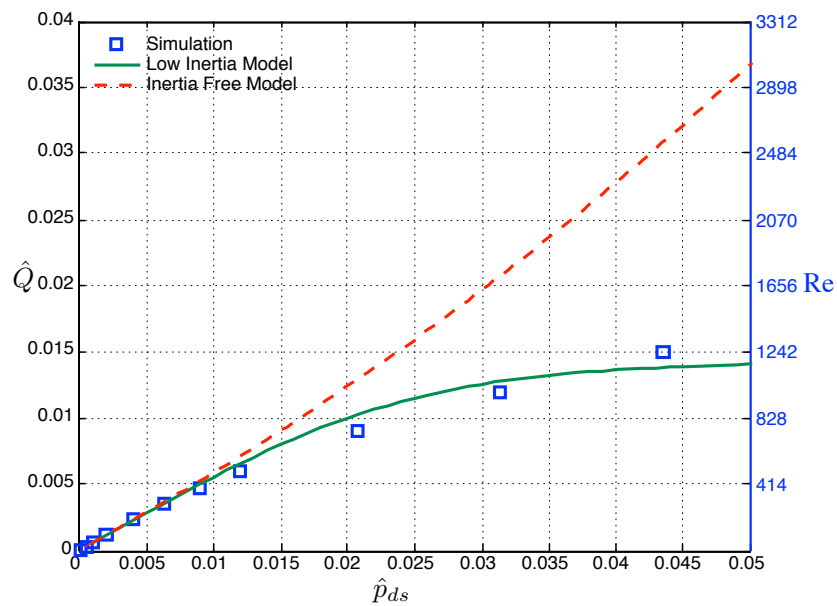

Figure 20: Comparison of the steady state flowrate $\hat{\mathbf{Q}}$ between the CFD simulation and the models

CHAPTER VI

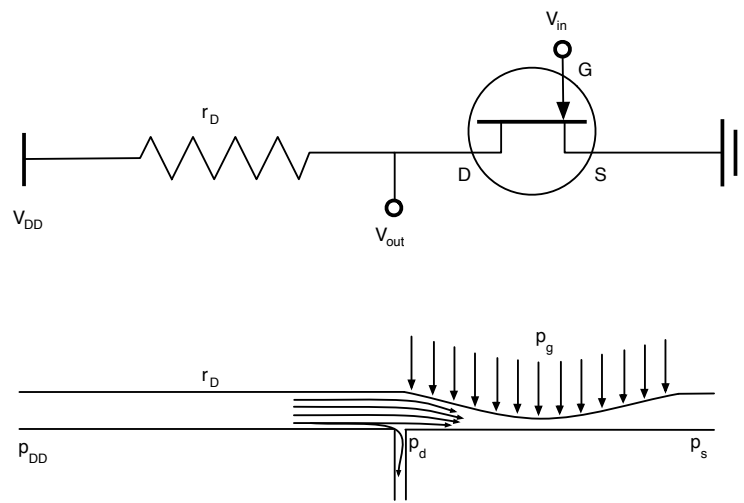# APPLICATIONS

A. Common Source Amplifier

Figure 21: Common Source Electrical Amplifier Circuit vs. Common Source Fluidic Circuit

In this section, we investigate the small signal transient behavior of the common-source configuration shown in Fig. 21. In electrical circuits the common-source amplifier is one of three basic single-stage field-effect transistor amplifier circuits, commonly used as a voltage amplifier. In common source circuits the input signal voltage enters the gate side of the MOSFET, changes the drain current and thus amplifies the drain voltage. A similar circuit can be achieved with microfluidics where a long channel is placed in stead of a resistor, and an alternating pressure is applied at the membrane acting as the input to the system, as show in Fig.21 The total gain of the microfluidic circuit is the product of the transconductance of the transistor g_m and the total output resistance; which is the intrinsic resistance r_o of the transistor in parallel to the resistance r_D of the channel. Accordingly, for small transient deflection of

the membrane, we get a total gain $\overline{A_v} = g_m(r_o||r_D)$ where g_m and r_o can be extracted form the simulation graphs presented previously or alternatively it can be obtained from the models. In our simulation to test the common source microfluidic circuit we used an entry and output channel length of 16000 μm and height 59 μm each, and membrane thickness of 195 μm. The pressure at the channel entry is $p_{DD} = 12000Pa$, the pressure at the exit of the channel is $p_s = 0$, and the input pressure applied at the top of the membrane is $p_g = 5500 + 500\sin(2\pi5t)$, all in gauge pressure.
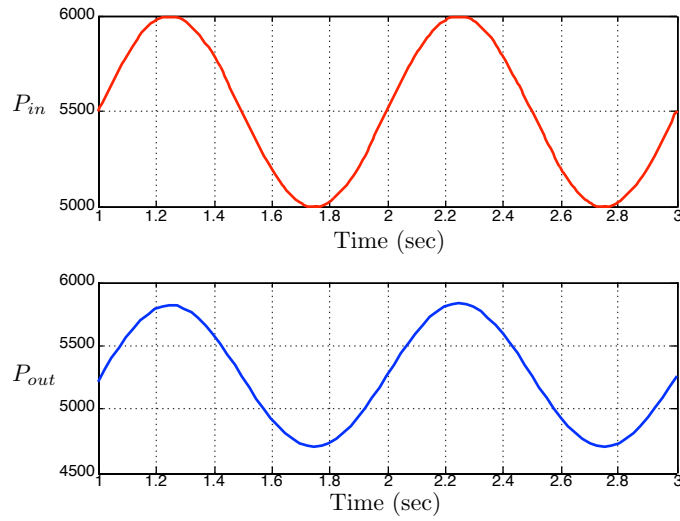

Figure 22: Input pressure applied at the membrane vs output pressure measured on the drain.

The pressure at input of the common source configuration p_g is plotted versus time along with the output channel i.e. p_d (drain of transistor), the applied external pressure in Fig. 22. It can be observed from Fig. 22 that p_d assumes a harmonic sinusoidal dependence on time, similar to p_g, which indicates that the device is linear, as expected from small signal behavior, and p_g/p_d which is the gain Av equals to 1.0.

The analysis can be extended for a range of frequencies to characterize the effect of frequency on gain for low frequencies. It is therefore noticed in Fig. 23 that the pressure gain has no dependence on the frequency for frequencies below a certain threshold for given "Re". However as the frequency increases above the critical value the gain will start to decrease. Note that this behavior can be also found in MOSFETs as
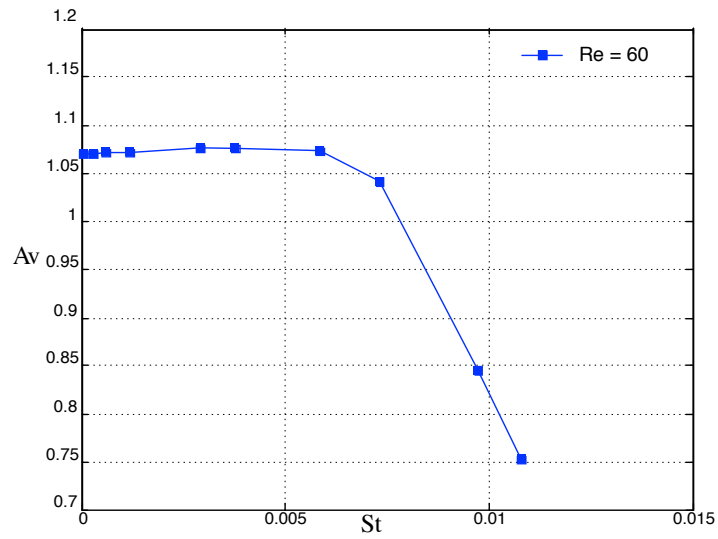
Figure 23: The change of Gain with respect to St

explained by Sedra and Smith in [17]. Such dynamics of a microfluidic transistor also puts limitations on its range of operation beyond which the gain A_v is not as predicted by the analytical equation.
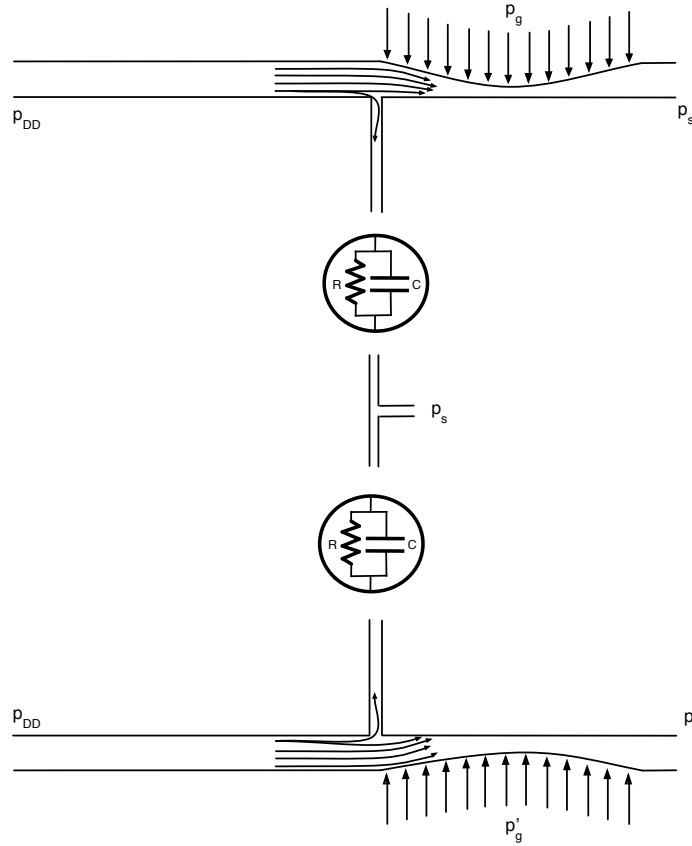
B. Mixing Circuit

Figure 24: Mixing Problem using the Common Source Configuration

The common source configuration implemented before can be used as a mixing application by connecting the output channel of two common source microfluidic circuits to a mixer channel as shown in Fig.24. Where the same pressure p_{DD} is applied at the entry but phase different pressures p_g & p'_g are applied at the input of the each transistor. The phase difference between the gain pressures of each transistor would create two, out of phase flows with the flow rates coming into the mixing channel equal to $Q = Q_{DC} + Q_{AC}$, where Q_{AC} is out of phase between the two flows. However since the magnitude of the alternating velocity $||Q_{AC}||$ is small compared to $||Q_{DC}||$ a micro-fluidic capacitor parallel to a resistor is added at the outlet of each channel to decrease the weight of the direct flow rate Q_{DC} entering the mixing channel. The capacitor in this circuit will allow only the AC component to pass and kills the DC while the resistor will

45

permit Q_{DC} to flow but lowers its magnitude. Thus using this circuit one can control the magnitude of the DC component of the flow rate as shown below:

$$Q'_{DC} = \frac{Q_{DC}R_O}{R_O + R}$$

where Q'_{DC} is the new DC component of the flow rate entering the mixing channel, Q_{DC} is the old DC component of the flow rate entering the device, R is the resistance of the device and R_O is the resistance of the output channel. So to decrease Q_{DC} by a factor of K, the resistor of the device would be equal to:

$$R = R_O(K - 1)$$

As for the capacitor, it should be designed with low impedance at the desired frequency f, with:

$$C > \frac{1}{2\pi f}$$

In our simulation we used the same configuration as the common source but made phase difference equal to $\pi/2$ between the two input pressures. Q_{DC} was decreased by a factor of 5, so since $R_O = 16000 \, \mu$ m, then the resistor that should be added in parallel to a capacitor would be equal to $R = 64000 \, \mu$ m. As for the capacitor, its capacitance should be greater than $1/(2\pi f)$ where f equals to 5Hz. The results of the simulation in Fig. 25 are shown at different time steps with respect to the period "T". As shown in the figure, mixing between the two flows entering the mixing channel is well

established throughout the channel

t = 0

t = 5 *T*/8

t = *T*/8

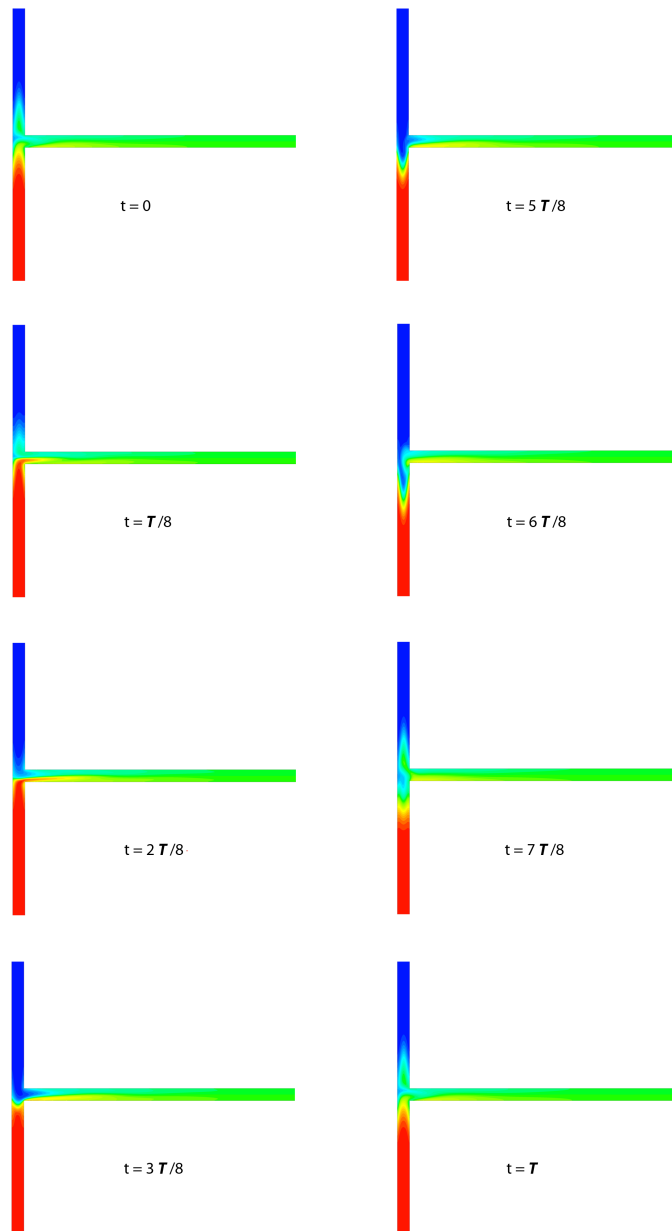t = 6 *T*/8

t = 2 *T*/8

t = 7 *T*/8

t = 3 *T*/8

t = *T*

Figure 25: Results for the mixing simulation

CHAPTER VII

CONCLUSION

A microfluidic analog flow controller is presented. A reduce order model for the device based on the governing equations is shown. Characterization of the deivce based on steady characteristic curves of the volume flowrate versus pressure drop and external pressure minus output pressure is presented in a manner analogous to $I_D - V_{GS}$ and $I_D - V_{DS}$ characteristic curves for a MOSFET. The reduced order model parameters (transconductance and intrinsic output resistance) in addition to the capacitive parameters can be derived numerically from the model or more accurately from simulation of the coupled fluid-structure problem. Extraction of these small signal parameters allows for fast small signal type analyses. Surprisingly, the transistive regime of the microfluidic controller is similar in many respects to its electronic MOSFET. Both have a square dependence of the current (volume flowrate) on the gate-source voltage (external pressure minus output pressure) in the long channel operation and a linear dependence in the short channel operation. Both also have a triode and saturation regime depending on the value of the pressure difference across the channel (V_{ds}). The benefits of accurate modeling and characterization of microfluidic transistors allows them to evolve from operating as binary on/off switches to analog component that can provide a variable gain. It is expected that this analog DC and small signal characterization will play an important role in future complex microfluidic devices as it offers accurate control of both amplitude and frequency of the pressure and volume flow rate.

BIBLIOGRAPHY

[1] Adams, M., Johnston, M., Scherer, A., Quake, S.: Polydimethylsiloxane based microfluidic diode. Journal of Micromechanics and Microengineering **15**(8), 1517 (2005)

[2] et. al, R.L.B.: Designing high-performance micro-pumps based on no-moving-parts valves. In: MicroElectroMechanical Systems (MEMS). The ASME International Mechanical Engineeing Congress and Exposition (1997)

[3] Bakarji, J.: A reduced order model of a microfluidic transistor. ASME Conference for Mechanical Engineering (2013)

[4] Begley, M.R.: The Mechanical Behavior of Films and Interfaces in Microfluidic Devices Implications for Performance and Reliability. Taylor and Francis Group, LLC (2008)

[5] Berthier, E., Beebe, D.J.: Flow rate analysis of a surface tension driven passive micropump. Lab on a Chip **7**(11), 1475–1478 (2007)

[6] Duffy, D.C., McDonald, J.C., Schueller, O.J., Whitesides, G.M.: Rapid prototyping of microfluidic systems in poly (dimethylsiloxane). Analytical chemistry **70**(23), 4974–4984 (1998)

[7] Grover, W.H., Ivester, R.H., Jensen, E.C., Mathies, R.A.: Development and

multiplexed control of latching pneumatic valves using microfluidic logical structures. Lab on a Chip **6**(5), 623–631 (2006)

[8] Jeon, N.L., Chiu, D.T., Wargo, C.J., Wu, H., Choi, I.S., Anderson, J.R., Whitesides, G.M.: Microfluidics section: design and fabrication of integrated passive valves and pumps for flexible polymer 3-dimensional microfluidic systems. Biomedical Microdevices **4**(2), 117–121 (2002)

[9] Kartalov, E.P., Walker, C., Taylor, C.R., Anderson, W.F., Scherer, A.: Microfluidic vias enable nested bioarrays and autoregulatory devices in newtonian fluids. Proceedings of the National Academy of Sciences **103**(33), 12,280–12,284 (2006)

[10] Kim, S.J.: Analyzing threshold pressure limitations in microfluidic transistors for self-regulated microfluidic circuits. Applied Physics Letters (2012)

[11] Leslie, D.C.: Frequency-specific flow control in microfluidic circuits with passive elastomeric features. Nature Physics **5** (2009)

[12] Mosadegh, B.: Integrated elastomeric components for autonomous refulation of sequential and oscillatory flow switching in microfluidic devices. Nature Physics **6**(433-437) (2010)

[13] Mosadegh, B.: Next-generation integrated microfluidic circuits. Lab Chip **11**(2813) (2011)

[14] Oh, K.W.: Design of pressure-driven microfluidic networks using elecric circuits analogies. Lab Chip (2011)

[15] Pennathur, S.: Flow control in microfluidics: are the workhorse flows adequate? Lab on a Chip **8**(3), 383–387 (2008)

[16] Rhee, M.: Microfluidic pneumatic logic circuits and digital pneumatic microprocessors for integrated microfluidic systems. Lab Chip **9**(3131-3143) (2009)

[17] Sedra, A.S.: Microelectonic Circuits. Oxford University Press (2004)

[18] Seiler, K., Fan, Z.H., Fluri, K., Harrison, D.J.: Electroosmotic pumping and valveless control of fluid flow within a manifold of capillaries on a glass chip. Analytical Chemistry **66**(20), 3485–3491 (1994)

[19] Senturia, S.D.: Mirosystem Design. Kluwer Academic Publishers (2002)

[20] Timoshenko, S., Woinowsky-Krieger, S., Woinowsky-Krieger, S.: Theory of plates and shells, vol. 2. McGraw-hill New York (1959)

[21] Toepke, M.: Microfluidic logic gates and timers. Lab Chip (2007)

[22] Toepke, M.W.: Microfluidic logic gates and timers. Lab Chip (2007)

[23] Utz, M.: Mirofluidic waves. Lab Chip (2011)

[24] Weaver, J.A.: Static control logic for microfluidic devices using pressure-gain valves. Nature Physics **6** (2010)

[25] Whitesides, G.M.: The origins and the future of microfluidics. Nature **442**(7101), 368–373 (2006)

[26] Yang, B., Lin, Q.: Planar micro-check valves exploiting large polymer compliance. Sensors and Actuators A: Physical **134**(1), 186–193 (2007)